Cell Metabolism

A Liver-Derived Secretory Protein, Selenoprotein P, Causes Insulin Resistance

Hirofumi Misu,[1,10] Toshinari Takamura,[1,10,*] Hiroaki Takayama,[1] Hiroto Hayashi,[1] Naoto Matsuzawa-Nagata,[1] Seiichiro Kurita,[1] Kazuhide Ishikura,[1] Hitoshi Ando,[1] Yumie Takeshita,[1] Tsuguhito Ota,[1] Masaru Sakurai,[1] Tatsuya Yamashita,[1] Eishiro Mizukoshi,[1] Taro Yamashita,[1] Masao Honda,[1] Ken-ichi Miyamoto,[2,3] Tetsuya Kubota,[4] Naoto Kubota,[4] Takashi Kadowaki,[4] Han-Jong Kim,[5] In-kyu Lee,[5] Yasuhiko Minokoshi,[6] Yoshiro Saito,[7] Kazuhiko Takahashi,[8] Yoshihiro Yamada,[9] Nobuyuki Takakura,[9] and Shuichi Kaneko[1]

[1]Department of Disease Control and Homeostasis

[2]Department of Hospital Pharmacy

[3]Department of Medicinal Informatics

Kanazawa University Graduate School of Medical Science, Kanazawa, Ishikawa 920-8641, Japan

[4]Department of Diabetes and Metabolic Diseases, Graduate School of Medicine, University of Tokyo, Tokyo 113-8655, Japan

[5]Section of Endocrinology, Department of Internal Medicine, Kyungpook National University Hospital, School of Medicine, Kyungpook National University, Jungu, Daegu 700-412, Korea

[6]Division of Endocrinology and Metabolism, Department of Developmental Physiology, National Institute for Physiological Sciences, Okazaki, Aichi 444-8585, Japan

[7]Department of Medical Life Systems, Faculty of Medical and Life Sciences, Doshisha University, Kyotanabe, Kyoto 610-0394, Japan

[8]Department of Nutritional Biochemistry, Hokkaido Pharmaceutical University, Otaru, Hokkaido 047-0264, Japan

[9]Department of Signal Transduction, Research Institute for Microbial Diseases, Osaka University, Osaka 565-0871, Japan

[10]These authors contributed equally to this work

*Correspondence: ttakamura@m-kanazawa.jp

DOI 10.1016/j.cmet.2010.09.015

SUMMARY

The liver may regulate glucose homeostasis by modulating the sensitivity/resistance of peripheral tissues to insulin, by way of the production of secretory proteins, termed hepatokines. Here, we demonstrate that selenoprotein P (SeP), a liver-derived secretory protein, causes insulin resistance. Using serial analysis of gene expression (SAGE) and DNA chip methods, we found that hepatic SeP mRNA levels correlated with insulin resistance in humans. Administration of purified SeP impaired insulin signaling and dysregulated glucose metabolism in both hepatocytes and myocytes. Conversely, both genetic deletion and RNA interference-mediated knockdown of SeP improved systemic insulin sensitivity and glucose tolerance in mice. The metabolic actions of SeP were mediated, at least partly, by inactivation of adenosine monophosphate-activated protein kinase (AMPK). In summary, these results demonstrate a role of SeP in the regulation of glucose metabolism and insulin sensitivity and suggest that SeP may be a therapeutic target for type 2 diabetes.

INTRODUCTION

Insulin resistance is an underlying feature of people with type 2 diabetes and metabolic syndrome (Saltiel and Kahn, 2001), but is also associated with risk for cardiovascular diseases (Després et al., 1996) and contributes to the clinical manifestations of nonalcoholic steatohepatitis (Ota et al., 2007). In an insulin-resistant state, impaired insulin action promotes hepatic glucose production and reduces glucose uptake by peripheral tissues, resulting in hyperglycemia. The molecular mechanisms underlying insulin resistance are not fully understood, but are now known to be influenced by the secretion of tissue-derived factors, traditionally considered separate from the endocrine system. Recent work in obesity research, for example, has demonstrated that adipose tissues secrete a variety of proteins, known as adipocytokines (Friedman and Halaas, 1998; Maeda et al., 1996; Scherer et al., 1995; Steppan et al., 2001; Yang et al., 2005), which can either enhance or impair insulin sensitivity, thereby contributing to the development of insulin resistance.

SeP (in humans encoded by the *SEPP1* gene) is a secretory protein primarily produced by the liver (Burk and Hill, 2005; Carlson et al., 2004). It contains ten selenocysteine residues and functions as a selenium supply protein (Saito and Takahashi, 2002). However, the role of SeP in the regulation of glucose metabolism and insulin sensitivity has not yet been established. Furthermore, the clinical significance of SeP in human diseases has not been well defined, although studies of SeP knockout mice showed SeP deficiency to be associated with neurological injury and low fertility (Hill et al., 2003; Schomburg et al., 2003).

The liver plays a central role in glucose homeostasis and is also the site for the production of various secretory proteins. For example, recent work in our laboratory has revealed that genes encoding secretory proteins are abundantly expressed in the livers of people with type 2 diabetes (Misu et al., 2007). Moreover, genes encoding angiogenic factors, fibrogenic factors, and redox-associated factors were differentially expressed in the livers of people with type 2 diabetes (Takamura et al., 2004; Takeshita et al., 2006), possibly contributing to the pathophysiology of

type 2 diabetes and its clinical manifestations. On the basis of these findings, we hypothesize that, analogous to adipose tissues, the liver may also contribute to the development of type 2 diabetes and insulin resistance, through the production of secretory proteins, termed hepatokines.

RESULTS

Identification of a Hepatic Secretory Protein Involved in Insulin Resistance

To identify hepatic secretory proteins involved in insulin resistance, we performed liver biopsies in humans and conducted a comprehensive analysis of gene expression profiles, using two distinct methods. First, we obtained human liver samples from five patients with type 2 diabetes and five nondiabetic subjects who underwent surgical procedures for malignant tumors, and we subjected them to serial analysis of gene expression (SAGE) (Velculescu et al., 1995). Consequently, we identified 117 genes encoding putative secretory proteins with expression levels in people with type 2 diabetes, 1.5-fold or greater higher than those in normal subjects. Next, we obtained ultrasonography-guided percutaneous needle liver biopsies from ten people with type 2 diabetes and seven normal subjects (Table S1 available online), and we subjected them to DNA chip analysis to identify genes whose hepatic expression was significantly correlated with insulin resistance (Table S2). We performed glucose clamp experiments on these human subjects and measured the metabolic clearance rate (MCR) of glucose (glucose infusion rate divided by the steady-state plasma glucose concentration) as a measure of systemic insulin sensitivity. As a result, we found that *SEPP1* expression levels were upregulated 8-fold in people with type 2 diabetes compared with normal subjects, as determined by SAGE (Table S2). Additionally, there was a negative correlation between hepatic *SEPP1* messenger RNA (mRNA) levels and the MCR of glucose, indicating that elevated hepatic *SEPP1* mRNA levels were associated with insulin resistance (Figure 1A). As a corollary, we found a positive correlation between the levels of hepatic *SEPP1* mRNA and postloaded or fasting plasma glucose (Figures 1B and 1C).

Elevation of SeP in Type 2 Diabetes

To characterize the role of SeP in the development of insulin resistance, we measured serum SeP levels in human samples (Table S3), using enzyme-linked immunosorbent assays (ELISA), as described previously (Saito et al., 2001). Consistent with elevated hepatic *SEPP1* mRNA levels, we found a significant positive correlation between serum SeP levels and both fasting plasma glucose and hemoglobin A_{1c} (HbA_{1c}) levels (Figures 1D and 1E). HbA_{1c} is a clinical marker of protein glycation due to hyperglycemia, and elevated HbA_{1c} levels generally reflect poor glucose control over a 2–3 month period. Additionally, serum levels of SeP were significantly elevated in people with type 2 diabetes compared with normal subjects (Figure 1F and Table S4). Similar to data derived from clinical specimens, in rodent models of type 2 diabetes, including OLETF rats and KKAy mice, hepatic *Sepp1* mRNA and serum SeP levels were elevated (Figures 1G–1J and Table S5).

SeP Expression in Hepatocytes Is Regulated by Glucose, Palmitate, and Insulin

To clarify the pathophysiology contributing to the hepatic expression of SeP in type 2 diabetes, we investigated the effects of nutrient supply on *Sepp1* mRNA expression in cultured hepatocytes. We found that the addition of glucose or palmitate upregulated *Sepp1* expression, whereas insulin downregulated it in a dose- and time-dependent manner (Figures 2A, 2C, 2E, and 2F). Similar effects on SeP protein levels were observed in primary mouse hepatocytes (Figures 2B, 2D, and 2G). Consistent with the negative regulation of *Sepp1* by insulin in hepatocytes, *Sepp1* mRNA levels were elevated in the livers of fasting C57BL6J mice, compared with those that had been fed (Figure 2H). Thus, multiple lines of evidence suggest that elevated SeP is associated with the development of insulin resistance.

SeP Impairs Insulin Signaling and Dysregulates Glucose Metabolism In Vitro

Because there is no existing cell culture or animal model in which SeP is overexpressed, we purified SeP from human plasma using chromatographic methods (Saito et al., 1999; Saito and Takahashi, 2002) to examine the effects of SeP on insulin-mediated signal transduction. Treatment of primary hepatocytes with purified SeP induced a reduction in insulin-stimulated phosphorylation of insulin receptor (IR), and Akt (Figures 3A and 3B). SeP exerts its actions through an increase in cellular glutathione peroxidase (Saito and Takahashi, 2002). Coadministration of BSO, a glutathione synthesis inhibitor, rescued cells from the inhibitory effects of SeP (Figure 3C). Moreover, SeP increased phosphorylation of IRS1 at Ser307, the downregulator of tyrosine phosphorylation of IRS (Figure S1A). Similar effects of SeP were also observed in C2C12 myocytes (Figure S1B). Next, we assessed whether SeP dysregulated cellular glucose metabolism. In H4IIHEC hepatocytes, treatment with SeP upregulated mRNA expression of *Pck1* and *G6pc*, key gluconeogenic enzymes, resulting in a 30% increase in glucose release in the presence of insulin (Figures 3D–3F). Treatment with SeP alone had no effects on the levels of mRNAs encoding gluconeogenic enzymes or on glucose production in the absence of insulin, suggesting that SeP modulates insulin signaling. Additionally, treatment with SeP induced a reduction in insulin-stimulated glucose uptake in C2C12 myocytes (Figure 3G). These in vitro experiments indicate that, at physiological concentrations, SeP impairs insulin signal transduction and dysregulated cellular glucose metabolism.

SeP Impairs Insulin Signaling and Disrupts Glucose Homeostasis In Vivo

To examine the physiological effects of SeP in vivo, we treated female C57BL/6J mice with two intraperitoneal injections of purified human SeP (1 mg/kg body weight), 12 and 2 hr before the experiments. Injection of purified human SeP protein resulted in serum levels of 0.5–1.5 μg/mL (data not shown). These levels correspond to the incremental change of SeP serum levels in people with normal glucose tolerance to those with type 2 diabetes (Saito et al., 2001). Glucose and insulin tolerance tests revealed that treatment of mice with purified SeP induced glucose intolerance and insulin resistance (Figures 3H and 3I). Blood insulin levels were significantly elevated in

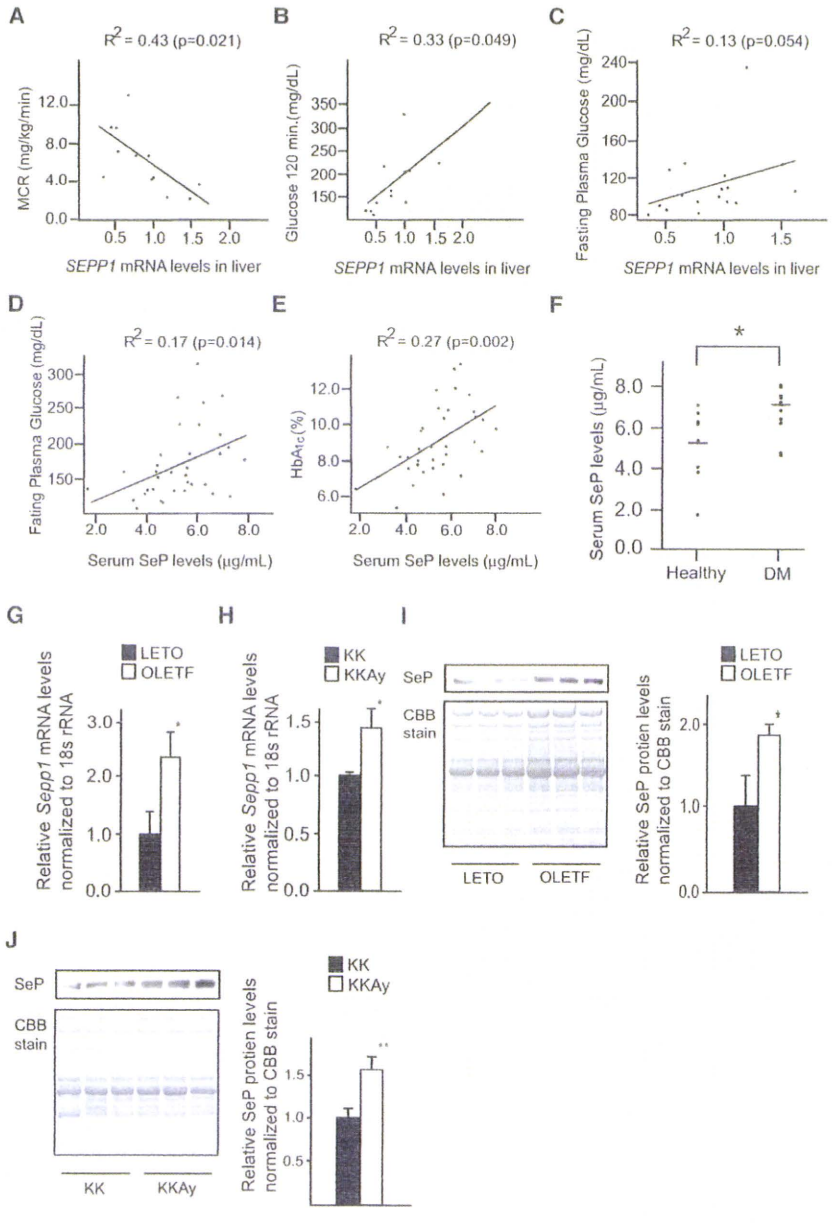

Figure 1. Elevation of Serum SeP Levels and Hepatic *Sepp1* Expression in Type 2 Diabetes

(A–C) Individual correlations between hepatic *SEPP1* mRNA levels and metabolic clearance rate (MCR) of glucose (A), postloaded plasma glucose levels (B), and fasting plasma glucose levels (C) in humans (n = 12–17). MCR equals the glucose infusion rate divided by the steady-state plasma glucose concentration, and is a measure of systemic insulin sensitivity. MCR values were determined by glucose clamp. *SEPP1* mRNA levels were quantified with DNA chips.

(D and E) Correlations between serum levels of SeP and fasting plasma glucose levels (D) and HbA_{1c} (E) in people with type 2 diabetes (n = 35).

(F) Serum levels of SeP in people with type 2 diabetes and healthy subjects (n = 9–12). Age and body weight were not significantly different between the two groups. Data represents the means ± SEM from two groups. $^*p < 0.05$.

(G and H) Hepatic *Sepp1* mRNA levels in an animal model of type 2 diabetes (n = 5–6).

(I and J) Serum SeP levels in an animal model of type 2 diabetes. SeP was detected by western blotting. Coomassie brilliant blue (CBB)-stained gel is used as a control for protein loading. Graphs display the results of densitometric quantification, normalized to CBB-stained proteins (n = 5).

Data represent the mean ± SEM from five to six mice per group. $^*p < 0.05$, $^{**}p < 0.01$. See also Tables S1–S5.

SeP-injected mice, although those of glucagon and GLP-1 were unaffected during a glucose tolerance test (Figure S1C). Western blot analysis showed a reduction in insulin-induced serine phosphorylation of Akt in both liver and skeletal muscle of SeP-injected mice (Figures 3J and 3K). Hyperinsulinemic-euglycemic clamp studies showed that treatment with SeP significantly increased endogenous glucose production and decreased peripheral glucose disposal (Figure S1D and Figures 3L and 3M). Additionally, serum levels of injected human SeP protein negatively correlated with rates of peripheral glucose disposal (Figure S1E). These data indicate that SeP impairs insulin signaling in the liver and skeletal muscle and induces glucose intolerance in vivo.

Knockdown of *Sepp1* in Liver Improves Glucose Intolerance and Insulin Resistance in Mice with Type 2 Diabetes

To determine whether knockdown of endogenous *Sepp1* enhances insulin signaling, we transfected H4IIEC hepatocytes with *Sepp1*-specific small interfering RNA (siRNA), and we observed a reduction in endogenous *Sepp1* mRNA and SeP protein levels (Figures 4A and 4B). Insulin-stimulated serine phosphorylation of Akt was enhanced in these treated cells (Figure 4C). Similarly, delivery of *Sepp1*-specific siRNAs into KKAy mice via a hydrodynamic transfection method (McCaffrey et al., 2002; Zender et al., 2003) resulted in a 30% reduction in SeP protein levels in the liver and blood (Figures 4D–4G and Figure S2). Knockdown of *Sepp1* improved both glucose intolerance (Figures 4H and 4I) and insulin resistance (Figures 4J and 4K) in KKAy mice.

SeP-Deficient Mice Show Improved Glucose Tolerance and Enhanced Insulin Signaling in Liver and Muscle

We further confirmed the long-term effects of lowered SeP using *Sepp1* knockout mice (Hill et al., 2003). SeP knockout mice were viable and displayed normal body weights when maintained on a selenium-sufficient diet. Body weight, food intake, and O_2 consumption were unaffected by SeP knockout (Figures S3A

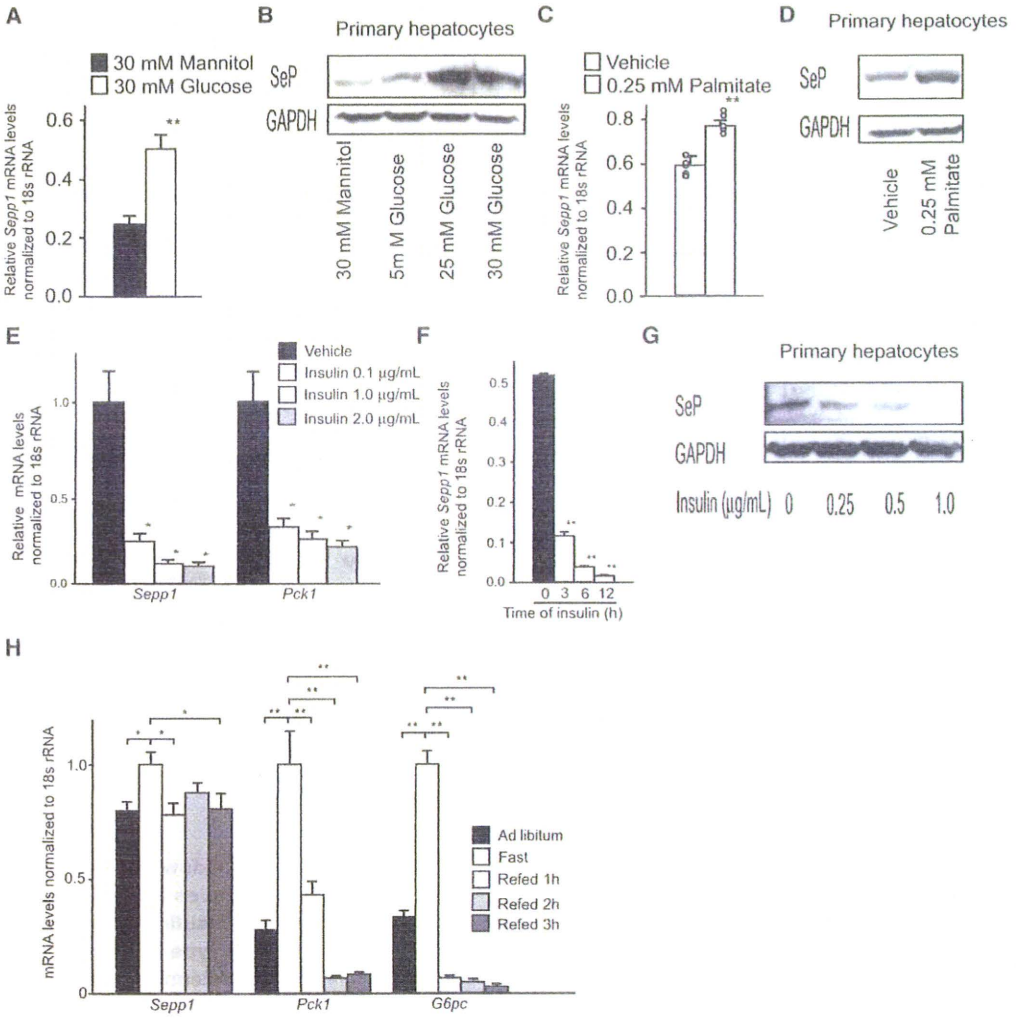

Figure 2. SeP Expression Is Regulated by Glucose, Palmitate, and Insulin

(A) *Sepp1* mRNA levels in H4IIEC hepatocytes treated with glucose or mannitol (30 mM) for 6 hr (n = 4).

(B) SeP protein levels in primary hepatocytes treated with glucose or mannitol for 6 hr.

(C) *Sepp1* mRNA levels in H4IIEC hepatocytes treated with palmitate (0.25 mM) for 16 hr (n = 5).

(D) SeP protein levels in primary hepatocytes treated with palmitate (0.25 mM) for 16 hr.

(E) *Sepp1* and *Pck1* mRNA levels in H4IIEC hepatocytes treated with various concentrations of insulin for 6 hr (n = 4).

(F) *Sepp1* mRNA levels in H4IIEC hepatocytes treated with insulin (0.1 μg/ml) for the indicated periods of time (n = 4).

(G) SeP protein levels in primary hepatocytes treated with various concentrations of insulin for 6 hr.

(H) Liver *Sepp1*, *Pck1*, and *G6pc* mRNA levels in C57BL/6J mice following fasting for 12 hr and subsequent refeeding (n = 4).

Data in (A), (C), (E), and (F) represent the means ± SEM from four to five cells per group, and data in (H) represent the means ± SEM from four mice per group. $^{*}p < 0.05$, $^{**}p < 0.01$.

and S3B). Lipid accumulation in the liver and adipose tissues was also unaffected (Figure 5A). However, postprandial plasma levels of insulin were reduced in *Sepp1*$^{-/-}$ mice, although blood glucose levels remained unchanged (Figures 5B and 5C). Glucose loading test revealed that *Sepp1*$^{-/-}$ mice showed improved glucose tolerance (Figure 5D). Insulin loading test revealed that *Sepp1*$^{-/-}$ mice showed lower blood glucose levels 60 min after insulin injection (Figure 5E). Insulin signaling, including phosphorylation of Akt and insulin receptor, was enhanced in the liver and skeletal muscle of *Sepp1*$^{-/-}$ mice (Figures 5F–5K). Additionally, *Sepp1*$^{+/-}$ tended to show enhanced insulin sensitivity. Plasma levels of glucagon, active GLP-1, and total GIP were unaffected by the loss of SeP in both fasted and fed mice (Figure S3C), suggesting that SeP dysregulated glucose metabolism in vivo primarily by modulating the insulin pathway, but not by affecting other hormones, including glucagon, GLP-1, and GIP.

SeP Deficiency Attenuates Adipocyte Hypertrophy and Insulin Resistance in Dietary Obese Mice

To determine whether SeP deficiency reduces insulin resistance caused by diet-induced obesity, we fed SeP knockout mice

a high-fat, high-sucrose diet (HFHSD) that is known to induce obesity, insulin resistance, and steatosis (Maeda et al., 2002). HFHSD tended to induce body weight gains in wild-type and *Sepp1*-deficient mice, although there was no significance between the three groups of animals (Figure 6A). Daily food intake was significantly increased in *Sepp1*$^{-/-}$ mice compared with wild-type animals (Figure 6B). Basal energy expenditure, as measured by O_2 consumption through indirect calorimetry, was also increased in *Sepp1*$^{-/-}$ mice (Figure 6C). Liver triglyceride content and epididymal fat mass were unaffected by *Sepp1* gene deletion (Figures S4A and 6D). However, diet-induced hypertrophy of adipocytes was attenuated in *Sepp1*$^{-/-}$ mice (Figures 6E and 6F and Figure S4B). Additionally, serum levels of free fatty acid and insulin were significantly reduced in these animals (Figures 6G–6I). Glucose and insulin loading tests revealed that *Sepp1*$^{-/-}$ mice were protected against glucose intolerance and insulin resistance even when on an obesity-inducing diet (Figures 6J and 6K).

SeP Reduces Phosphorylation of AMPKα Both In Vitro and In Vivo

Adenosine monophosphate-activated protein kinase (AMPK) is a serine/threonine kinase that phosphorylates a variety of energy-associated enzymes and functions as a metabolic regulator that promotes insulin sensitivity (Kahn et al., 2005). In this study, we found that SeP treatment reduced phosphorylation of AMPKα and ACC in both H4IIEC hepatocytes and mouse liver (Figures S5A and 7A). Fatty acid β oxidation and β oxidation-related gene expression were also suppressed by SeP (Figures S5B–S5D). The levels of AMP and ATP were unchanged in hepatocytes treated with SeP (Figure S5E). In contrast, *Sepp1*-deficient mice exhibited increased phosphorylation of AMPKα and ACC in the liver (Figure 7B). To determine whether AMPK pathways were involved in the action of SeP, we infected H4IIEC hepatocytes with an adenovirus encoding dominant-negative (DN) or constitutively active (CA) AMPK. Transduction with DN-AMPK reduced insulin-stimulated Akt phosphorylation such that it could not be further decreased by SeP (Figures 7C–7E). In contrast, when CA-AMPK was overexpressed, SeP was unable to impair insulin-stimulated Akt phosphorylation (Figures 7F–7H). Additionally, coadministration of 5-aminoimidazole-4-carboxyamide ribonucleoside (AICAR), a known activator of AMPK, rescued cells from the inhibitory effects of SeP on insulin signaling (Figure 7I). These results suggest that reduced phosphorylation of AMPK mediates, at least in part, the inhibitory effects of SeP on insulin signal transduction. Next, we examined the effects of SeP on some of the proteins that regulate the phosphorylation of AMPK. SeP dose-dependently increased the levels of protein phosphatase 2C (PP2C), a negative regulator of AMPK phosphorylation, in H4IIEC hepatocytes (Figure 7J). Expression of LKB1 and CaMKKβ, two positive regulators of AMPK, was unaffected by SeP treatment.

DISCUSSION

A Liver-Derived Secretory Protein, SeP, Causes Insulin Resistance

Our research reveals that hepatic overproduction of SeP contributes to the development of insulin resistance in the liver and skeletal muscle (Figure S5F). The liver plays a central role in glucose homeostasis, mainly via glycogen storage and glucose release into the blood stream. In addition, the liver is a major site for the production of secretory proteins. Therefore, we hypothesized that the liver would maintain glucose homeostasis by producing liver-derived secretory protein(s) termed hepatokines. In fact, several studies have shown that hepatic secretory factors, including the angiopoietin-like protein family (Oike et al., 2005; Xu et al., 2005) and fetuin-A (Auberger et al., 1989; Srinivas et al., 1993), are involved in insulin sensitivity. However, we speculated that the identification of the liver-derived proteins that directly contribute to the pathogenesis of insulin resistance or type 2 diabetes may not be adequate. Specifically, our comprehensive approach using global gene expression analyses revealed that numerous genes encoding secretory proteins are expressed and altered in the human type2 diabetic liver (Misu et al., 2007). Thus, by comparing the expression levels and clinical parameters for glycemic control and insulin resistance, we selected candidate genes for liver-produced secretory proteins that cause insulin resistance. The current study sheds light on a previously underexplored function of the liver that is similar to adipose tissue; the liver may participate in the pathogenesis of insulin resistance through hormone secretion.

Suppression of SeP Expression by Insulin in Hepatocytes

Our results indicate that insulin negatively regulates SeP expression in hepatocytes. These findings are consistent with recent reports that the SeP promoter is a target of FoxO (forkhead box, class O) and PGC-1α (peroxisome proliferator-activated receptor-γ coactivator 1α), both of which are negatively regulated by insulin in hepatocytes (Speckmann et al., 2008; Walter et al., 2008). Consistent with these findings in vitro, we showed that hepatic SeP expression was upregulated in mice in the fasting state. Under hypoinsulinemic conditions, such as a fasting state, upregulation of SeP might prevent hypoglycemia by decreasing glucose uptake in peripheral tissues and by increasing hepatic glucose production. Our results raise the possibility that the liver regulates systemic insulin sensitivity by sensing blood insulin levels and altering the production of SeP.

SeP Decreases Phosphorylation of AMPK and ACC in Hepatocytes

Identification of SeP receptor(s) in insulin-target organs is necessary to clarify the action mechanisms of SeP. Several lines of evidence have shown that apolipoprotein E receptor 2 (ApoER2) functions as an SeP receptor in the testis (Olson et al., 2007) and brain (Burk et al., 2007), both by acting as a cellular uptake receptor and by inducing intracellular signaling (Masiulis et al., 2009). It remains unknown whether ApoER2 acts as the SeP receptor in the liver or skeletal muscle. However, in this study, technical difficulties in the identification of a SeP receptor(s) led us to screen for well-established pathways associated with metabolic derangement to clarify the specific mechanisms of SeP action. As a result, our experiments reveal that SeP reduces phosphorylation of AMPK and its target ACC in H4IIEC hepatocytes and the livers of C57BL6J mice, possibly in an AMP/ATP ratio-independent manner. AMPK functions as a regulator of

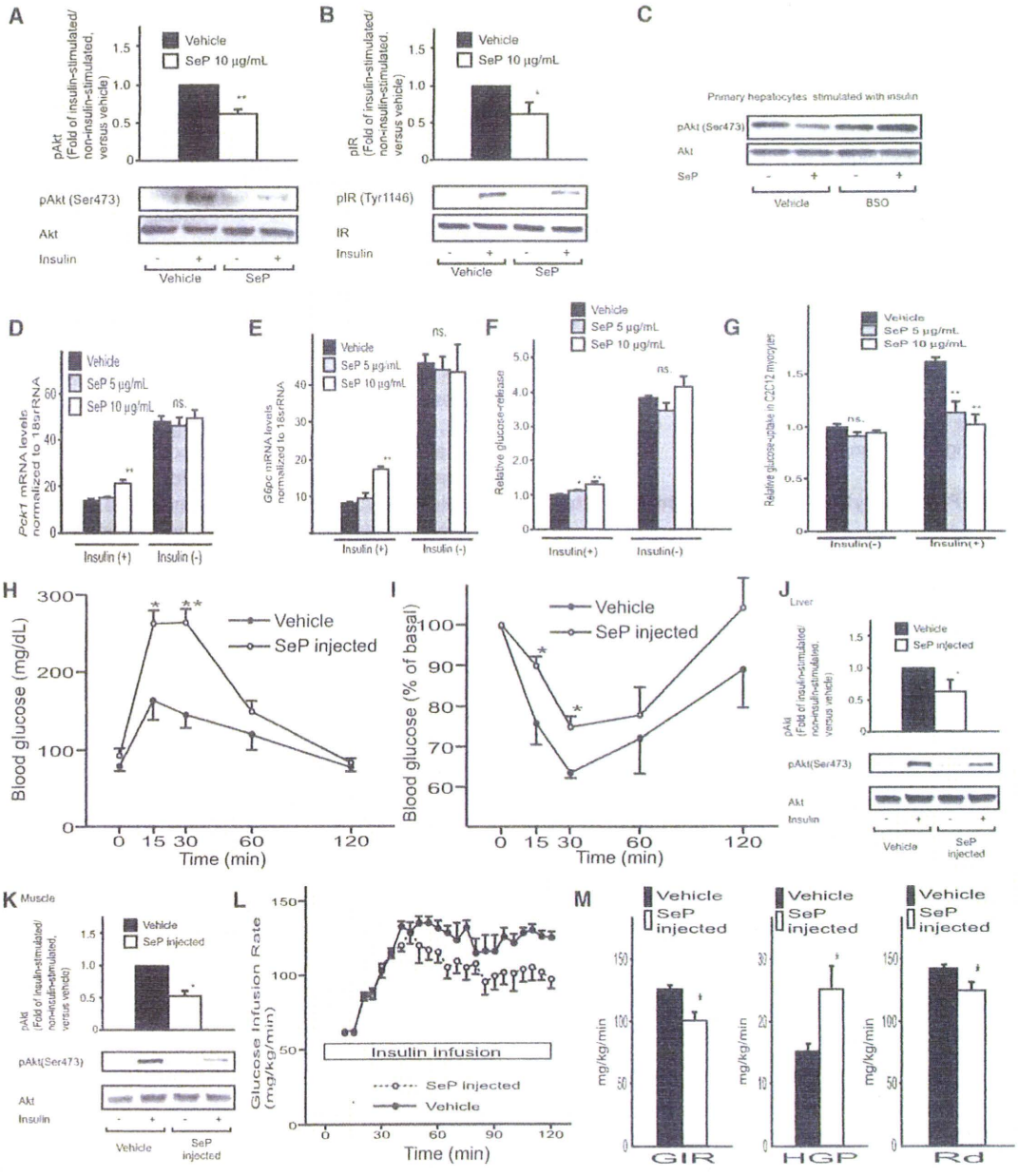

Figure 3. SeP Impairs Insulin Signaling In Vitro and In Vivo

(A and B) Effects of SeP on serine phosphorylation of Akt (A) and tyrosine phosphorylation of insulin receptor (B) in insulin-stimulated primary hepatocytes. Data represent the means ± SEM of three independent experiments. $^{*}p < 0.05$, $^{**}p < 0.01$ (versus vehicle-treated cells). Primary hepatocytes were treated with SeP or vehicle for 24 hr, and then the cells were stimulated with 1 ng/ml insulin for 15 min.

(C) Effects of BSO on SeP-induced changes in insulin-stimulated Akt phosphorylation in primary hepatocytes.

(D and E) Effects of SeP on the expression of mRNAs encoding gluconeogenic enzymes in H4IIEC hepatocytes (n = 5).

(F) Release of glucose from H4IIEC hepatocytes treated with SeP for 24 hr (n = 6).

(G) Effects of SeP on glucose uptake in C2C12 myocytes (n = 6).

(H and I) Glucose (H) and insulin (I) tolerance tests in mice injected with SeP or vehicle (n = 5). Glucose (1.5 g/kg body weight) and insulin (0.5 unit/kg body weight) were administered intraperitoneally.

(J and K) Effects of SeP on serine phosphorylation of Akt in liver (J) and skeletal muscle (K) in mice injected with purified human SeP or vehicle. Mice (n = 3 or 4) were stimulated with insulin (administered intraperitoneally). At 20 min after insulin stimulation, mice were anesthetized, and liver and hind-limb muscle samples removed for analysis.

(L) Time course of glucose infusion rate (GIR) during hyperinsulinemic-euglycemic clamp in mice injected with SeP or vehicle (n = 6).

(M) GIR, endogenous glucose production (EGP), and rate of glucose disposal (Rd) during hyperinsulinemic-euglycemic clamp (n = 6).

cellular energy homeostasis (Kahn et al., 2005) and mediates some effects of peripheral hormones such as leptin (Minokoshi et al., 2002) and adiponectin (Yamauchi et al., 2002); however, the mechanisms by which these adipokines alter AMPK phosphorylation are not fully understood. Our present findings demonstrate that SeP increases the levels of PP2C in H4IIEC hepatocytes. PP2C is a phosphatase that inactivates AMPK by dephosphorylating a threonine residue (Thr172) that lies in its α-catalytic subunit (Davies et al., 1995). Tumor necrosis factor α (TNF-α), a representative inflammatory cytokine linked to insulin resistance, is known to reduce AMPK phosphorylation by upregulating PP2C (Steinberg et al., 2006). Similar to TNF-α, SeP may reduce AMPK phosphorylation, at least partly, by upregulating PP2C. Further characterization of SeP and SeP-receptor-mediated interactions will provide insights into the involvement of SeP in PP2C upregulation and AMPK dephosphorylation.

Mechanism Underlying SeP-Mediated Insulin Resistance Varies between Liver and Skeletal Muscle

Given that plasma SeP is derived mainly from the liver (Carlson et al., 2004), our results suggest that AMPK mediates, at least in part, the autocrine/paracrine action of SeP. One limitation of our study is that the mechanism by which SeP acts on skeletal muscle remains unknown. Unlike in the liver, SeP-induced inhibitory effects on AMPK were not observed in either the skeletal muscle of C57BL6J mice or C2C12 myocytes (data not shown). Additionally, we showed that SeP reduces tyrosine phosphorylation of insulin receptors in primary hepatocytes. In contrast, SeP acts on serine phosphorylation of IRS1, but not tyrosine phosphorylation of insulin receptors, in C2C12 myocytes (data not shown). These results suggest that SeP disrupts the insulin signal cascade at different levels between hepatocytes and myocytes. SeP might induce insulin resistance in skeletal muscle, possibly through AMPK-independent pathways. The mechanisms that connect SeP to insulin resistance likely exhibit tissue specificity.

We showed that SeP heterozygous mice have no phenotype in glucose- and insulin-loading tests, whereas a 30% decrease in SeP levels caused by the injection of siRNA improves glucose tolerance and insulin resistance in KKAy mice. In general, multiple compensatory changes are observed in knockout mice, because the target gene has been absent since conception. In contrast, compensation may be inadequate in adult animals in which the target gene has been knocked down with siRNA. In fact, real-time PCR analysis showed that expression of the gene encoding IL-6, a representative inflammatory cytokine linked to insulin resistance, shows compensatory upregulation in the liver of *Sepp1*$^{-/+}$ mice, but not in *Sepp1* siRNA-treated KKAy mice (data not shown). Induction of IL-6 might compensate for the 50% reduction in SeP levels in *Sepp1*$^{-/+}$ mice.

Actions of SeP on the central nervous system may contribute to the in vivo phenotype. We did find that SeP-deficient mice fed a high-fat, high-sucrose diet display increases in food intake and O2 consumption (Figures 6B and 6C), suggesting that SeP acts on the central nervous system. Additionally, an earlier report described the colocalization of SeP and amyloid-β protein in the brains of people with Alzheimer's disease, suggesting the potential involvement of SeP in this condition's pathology (Bellinger et al., 2008). More recently, Takeda et al. reported that amyloid pathology in Alzheimer's disease may adversely affect diabetic phenotypes in mice (Takeda et al., 2010). Further experiments are necessary to determine whether the actions of SeP on the central nervous system involve the in vivo phenotype seen in this study.

We cannot exclude the possibility that the current phenotype in *Sepp1*-deficient mice is affected by the abnormal distribution of selenium. In fact, selenium levels in plasma and several tissues have been reported to be reduced in *Sepp1*-deficient mice fed a selenium-restricted diet (Schomburg et al., 2003). However, Burk et al. reported that the selenium levels in all tissues except the testis were unchanged in these mice fed a diet containing adequate amounts of selenium (Hill et al., 2003). In this study, we performed experiments using *Sepp1*-deficient mice fed a diet containing adequate amounts of selenium. Thus, we speculate that the effects of abnormal selenium distribution on our results in *Sepp1*-deficient mice may be insignificant.

A limitation of this study is that we could not match age, gender, or body weight completely between people with type 2 diabetes and normal subjects when comparing the serum SeP levels, as a result of the limited sample numbers. However, a previous large-scale clinical report showed that the age-, gender-, race-, and BMI-adjusted mean serum selenium levels were significantly elevated in participants with diabetes compared with those without diabetes in the US population (Bleys et al., 2007). Additionally, several lines of evidence showed that serum selenium levels are positively correlated with those of SeP in humans (Andoh et al., 2005; Persson-Moschos et al., 1998). In combination with our result, these reports lead us to speculate that serum SeP levels are also elevated in people with type 2 diabetes compared with normal subjects. However, additional large-scale clinical trials are needed to address this.

In summary, our experiments have identified SeP as a liver-derived secretory protein that induces insulin resistance and hyperglycemia. Our findings suggest that the secretory protein SeP may be a target for the development of therapies to treat insulin resistance-associated diseases, including type 2 diabetes.

EXPERIMENTAL PROCEDURES

Animals

Eight-week-old c57BL/6J mice were obtained from Sankyo Lab Service (Tokyo, Japan). Male Otsuka Long-Evans Tokushima Fatty (OLETF) rats and Long-Evans Tokushima Otsuka (LETO) rats were obtained from the Otsuka Pharmaceutical Tokushima Research Institute (Tokushima, Japan). OLETF

C57BL/6J mice were twice injected intraperitoneally with purified human SeP (1 mg/kg body weight) or vehicle in (H)–(M). Injections were administered 12 and 2 hr before the each experiment. Data in (D)–(G) represent the means ± SEM from five to six cells per group, and data in (H)–(M) represent the means ± SEM from three to six mice per group. $^{*}p < 0.05$, $^{**}p < 0.01$ versus cells treated with vehicle in (D)–(G). $^{*}p < 0.05$, $^{**}p < 0.01$ versus mice treated with vehicle in (H)–(M). See also Figure S1.

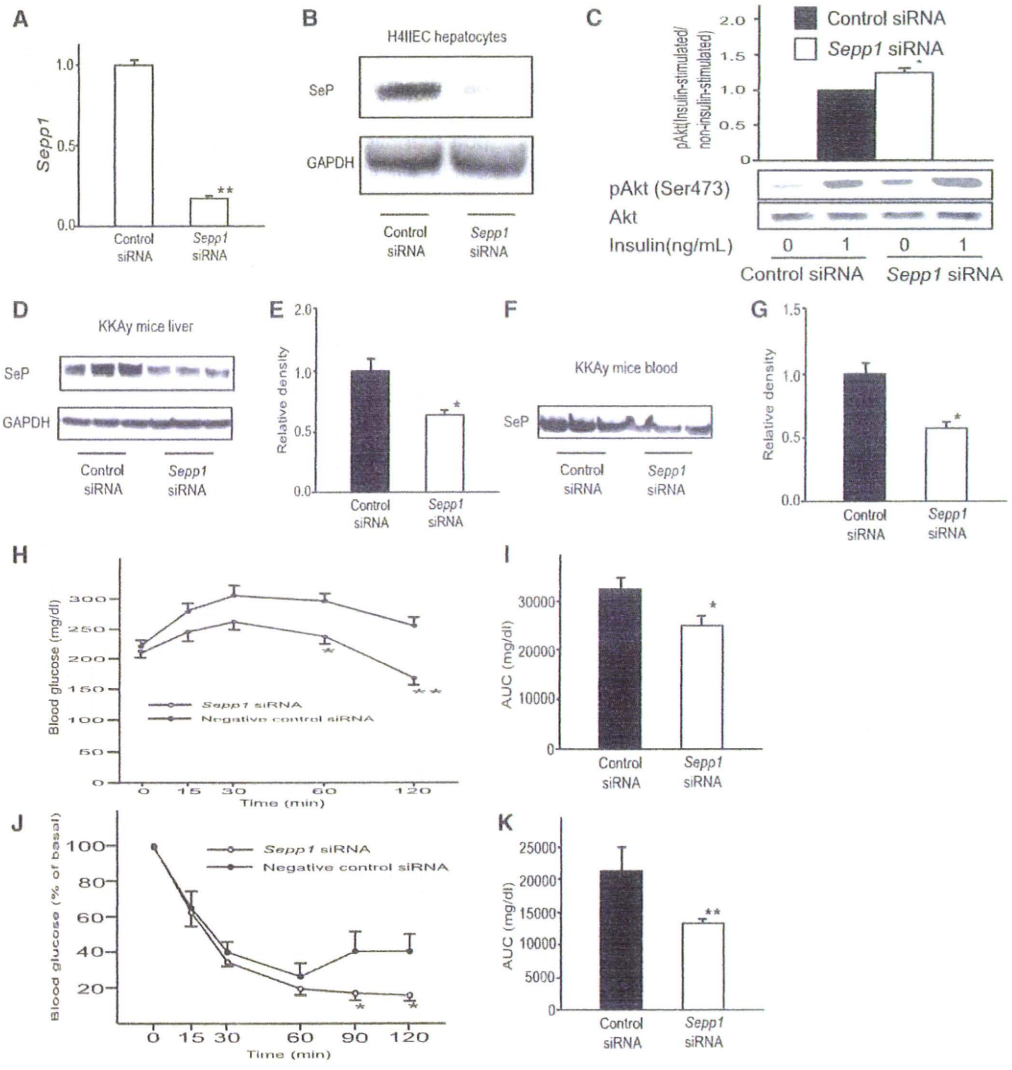

Figure 4. *Sepp1* Knockdown in the Liver Improves Insulin Sensitivity

(A) *Sepp1* mRNA levels in H4IIEC hepatocytes transfected with control or *Sepp1*-specific siRNA (n = 4).

(B) SeP protein production in H4IIEC hepatocytes transfected with *Sepp1*-specific siRNA. SeP production was detected in whole cell lysates by western blotting.

(C) Effects of SeP knockdown on insulin-stimulated serine phosphorylation of Akt in H4IIEC hepatocytes. Data represent the mean ± SEM of three independent experiments.

(D and E) Liver SeP production in KKAy mice injected with control or *Sepp1*-specific siRNA (n = 6). SeP protein levels were measured by western blotting 4 days after injection of siRNA.

(F and G) Blood SeP levels in KKAy mice injected with siRNA. Blood samples were obtained 4 days after siRNA injection (n = 6).

(H–K) Intraperitoneal glucose (H and I) and insulin (J and K) tolerance tests in KKAy mice (n = 6–8) injected with control or *Sepp1*-specific siRNA. Glucose and insulin was administered at doses of 0.3 g/kg body weight and 4 units/kg body weight, respectively.

Area under the curve (AUC) for blood glucose levels is shown in (I) and (K). Data in (A) represent the means ± SEM from four cells per group, and data in (E) and (G)–(K) represent the means ± SEM from six to eight mice per group. $^{*}p < 0.05$ versus cells transfected with control siRNA in (A) and (C). $^{*}p < 0.05$, $^{**}p < 0.01$ versus mice injected with control siRNA in (E) and (G)–(K). See also Figure S2.

rats have been established as an animal model of obesity-related type 2 diabetes (Kawano et al., 1992). Female KKAy mice were obtained from CLEA Japan (Tokyo, Japan). All animals were housed in a 12 hr light/dark cycle and allowed free access to food and water. High-fat and high-sucrose diet (D03062301) was purchased from Research Diets (New Brunswick, NJ). The experiments with OLETF and LETO rats were performed with frozen blood and liver samples obtained in our previous study (Ota et al., 2007).

Purification of SeP

SeP was purified from human plasma via conventional chromatographic methods, as previously described (Saito et al., 1999; Saito and Takahashi, 2002). Homogeneity of purified human SeP was confirmed by analysis of both amino acid composition and sequence (Saito et al., 1999). Concentrations of purified SeP were measured by the Bradford method, using bovine immunoglobulin G as a standard.

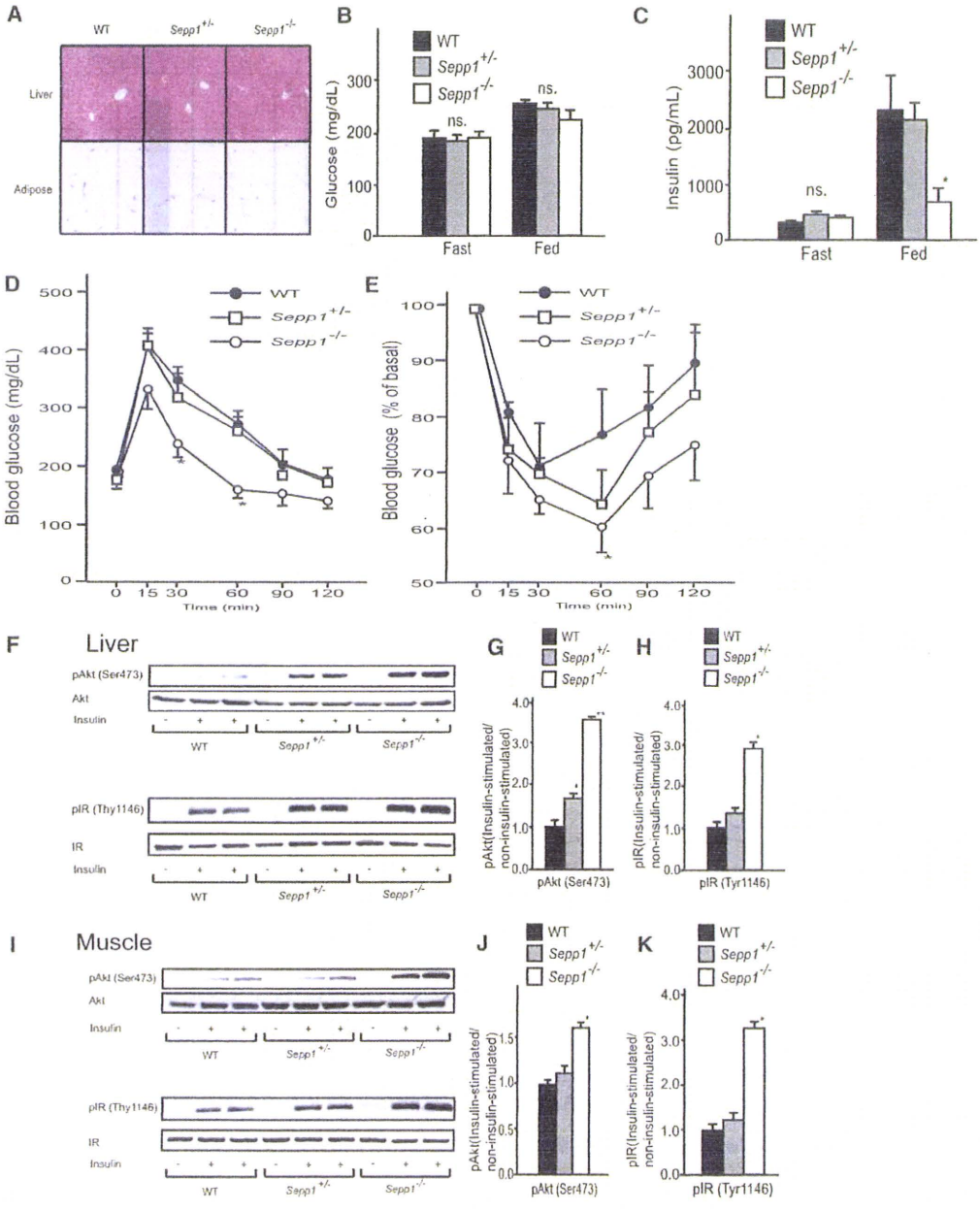

Figure 5. *Sepp1*-Deficient Mice Show Improved Glucose Tolerance and Enhanced Insulin Sensitivity

(A) Hematoxylin-and-eosin-stained liver and epididymal fat sections from male *Sepp1*$^{+/-}$ and *Sepp1*$^{-/-}$ mice.

(B) Blood glucose levels in *Sepp1*-deficient mice (n = 7). The mice were fasted for 6 hr.

(C) Blood insulin levels in *Sepp1*-deficient mice (n = 7).

(D and E) Intraperitoneal glucose (D) and insulin (E) tolerance tests in male *Sepp1*-deficient mice (n = 7). Glucose and insulin were administered at doses of 1.5 g/kg body weight and 4 units/kg body weight, respectively.

(F–K) Western blot analysis of phosphorylated Akt (pAkt) and phosphorylated insulin receptor (pIR) in liver (F–H) and skeletal muscle (I–K). Mice (n = 6) were stimulated with insulin (administered intraperitoneally). At 20 min after insulin stimulation, mice were anesthetized, and liver and hind-limb muscle samples removed for analysis.

Data in (B)–(E), (G), (H), (J), and (K) represent the means ± SEM from six to seven mice per group. *$p < 0.05$, **$p < 0.01$ versus wild-type mice. See also Figure S3.

siRNA Injection into KKAy mice

Delivery of siRNA targeted to the liver was performed by tail vein injections into mice, via hydrodynamic techniques, as previously described (McCaffrey et al., 2002; Zender et al., 2003). For these experiments, KKAy mice at 7–8 weeks of age (31–33 g body weight) were used. Mice were anesthetized with pentobarbital, and 2 nmol of siRNA, diluted in 3 ml of PBS, was injected into the tail vein over 15–20 s. All siRNAs were purchased from Applied Biosystems (Silencer^{R} In Vivo Ready Pre-designed siRNA). *Sepp1* siRNAs with the following

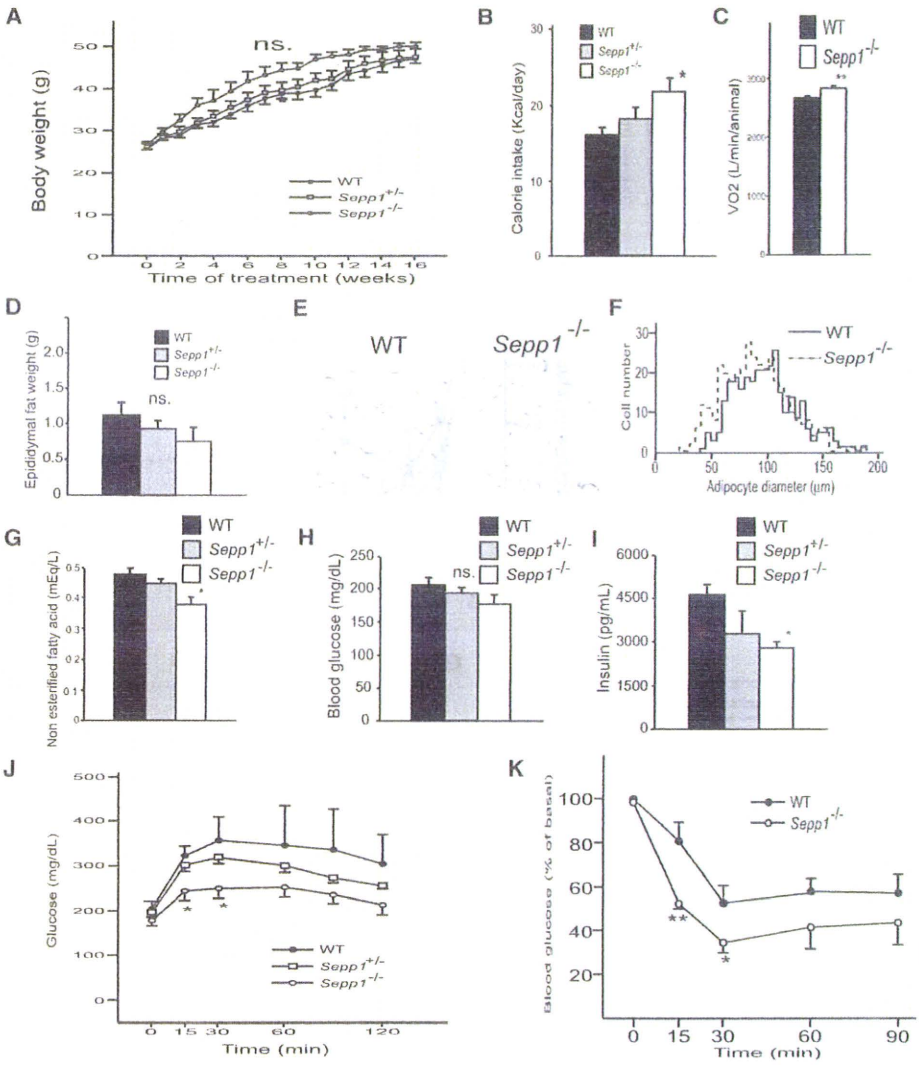

Figure 6. *Sepp1*-Deficient Mice Are Protected from Diet-Induced Insulin Resistance and Adipocyte Hypertrophy

(A) Body weight of *Sepp1*-deficient and wild-type mice fed a high-fat, high-sucrose diet (HFHSD; n = 4–8). Sixteen-week-old male mice were fed a HFHSD for 16 weeks.

(B) Daily calorie intake in *Sepp1*-deficient and wild-type mice (n = 4–8).

(C) Energy expenditure (as measured by VO_2 consumption through indirect calorimetry; n = 4).

(D) Epididymal fat mass in *Sepp1*-deficient and wild-type mice fed HFHSD (n = 4–7).

(E) Hematoxylin-and-eosin-stained epididymal fat sections from wild-type and *Sepp1*$^{-/-}$ mice.

(F) Histogram showing adipocyte diameters. We determined adipocyte diameters by measuring at least 300 adipocytes randomly selected from four independent sections.

(G) Blood nonestimated fatty acid levels in *Sepp1*-deficient and wild-type mice fed HFHSD (n = 4–7).

(H) Blood glucose levels in *Sepp1*-deficient and wild-type mice fed HFHSD (n = 4–8).

(I) Blood insulin levels in *Sepp1*-deficient and wild-type mice fed HFHSD (n = 4–8). Blood samples were obtained from mice fed a HFHSD for 16 weeks after a 12 hr fast in (G)–(I).

(J) Intraperitoneal glucose tolerance tests in wild-type and *Sepp1*-deficient mice (n = 4–8). Glucose was administered at a dose of 0.3 g/kg body weight.

(K) Intraperitoneal insulin tolerance tests in wild-type and *Sepp1*-deficient mice (n = 5–10). Insulin was administered at a dose of 2.0 units/kg body weight.

Data in (A)–(D) and (G)–(K) represent the means ± SEM from four to ten mice per group. $^{*}p < 0.05$, $^{**}p < 0.01$ versus wild-type mice. See also Figure S4.

sequence were synthesized: mouse *Sepp1*, 5′-GGUGUCAGAACACAUC GCAtt-3′ (sense). Negative control siRNA was also used and had no significant homology with any known gene sequences in mouse, rat, or human. Glucose and insulin loading tests were performed 2–7 days after injection of mice with siRNA.

SeP Knockout Mice

SeP knockout mice were produced by homologous recombination with genomic DNA cloned from an Sv-129 P1 library, as described previously (Hill et al., 2003). As female SeP knockout mice had inconsistent phenotypes, only male mice were used in this study.

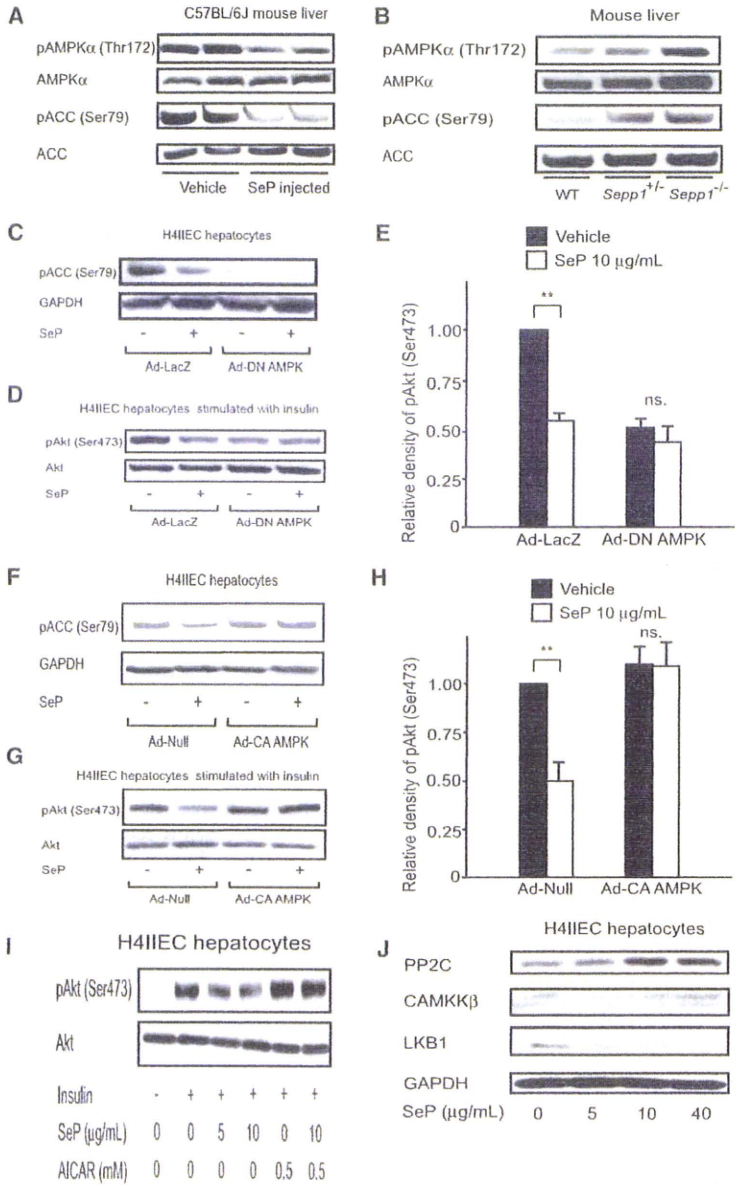

Figure 7. SeP Reduces Phosphorylation of AMPK and ACC in Hepatocytes

(A) Phosphorylation of AMPK and ACC in the liver of mice injected with SeP or vehicle. C57BL/6J mice were injected intravenously with purified human SeP (1 mg/kg body weight) or vehicle (phosphate-buffered saline). At 6 hr after injection, the liver was removed.

(B) Phosphorylation of AMPK and ACC in the liver of *Sepp1*-deficient mice after a 12 hr fast.

(C–E) Effects of dominant-negative AMPK on ACC phosphorylation (C) and insulin-stimulated Akt phosphorylation (D and E) in H4IIEC hepatocytes treated with SeP.

(F–H) Effects of constitutively active AMPK on ACC phosphorylation (F) and insulin-stimulated Akt phosphorylation (G and H) in H4IIEC hepatocytes treated with SeP.

(I) Effect of AICAR on SeP-induced insulin resistance in H4IIEC hepatocytes.

(J) Levels of PP2C, CaMKKβ, and LKB1 in H4IIEC hepatocytes treated with various concentrations of SeP for 12 hr.

Data in (E) and (H) represent the means ± SEM from three independent experiments. $^{**}p < 0.01$ versus vehicle-treated cells. See also Figure S5.

Statistical Analyses

All data were analyzed using the Japanese Windows Edition of the Statistical Package for Social Science (SPSS) Version 11.0. Numeric values are reported as the mean ± SEM. Differences between two groups were assessed with unpaired two-tailed t tests. Data involving more than two groups were assessed by analysis of variance (ANOVA). Glucose and insulin tolerance tests were examined with repeated-measures ANOVA.

ACCESSION NUMBERS

Microarray data have been deposited in Gene Expression Omnibus under accession number GSE23343.

SUPPLEMENTAL INFORMATION

Supplemental Information includes Supplemental Experimental Procedures, five figures, and five tables and can be found with this article online at doi:10.1016/j.cmet.2010.09.015.

ACKNOWLEDGMENTS

We thank Kuniaki Arai of Kanazawa University for liver biopsies and Isao Usui, Hajime Ishihara, and Toshiyasu Sasaoka of Toyama University for supplying their technical expertise on Western blot analyses of phosphoproteins. We thank Yuriko Furuta and Yoko Hashimoto for technical assistance. We thank Fabienne Foufelle of Université Pierre et Marie Curie for providing adenovirus vector encoding DN-AMPK. We are indebted to Kristina E. Hill and Raymond F. Burk of Vanderbilt University School of Medicine for the *Sepp1* knockout mice. This work was supported by Takeda Science Foundation and Grants-in-Aid from the Ministry of Education, Culture, Sports, Science and Technology, Japan. We also thank Cathie Chung for editing the manuscript.

Received: February 2, 2009
Revised: April 29, 2010
Accepted: August 13, 2010
Published: November 2, 2010

REFERENCES

Andoh, A., Hirashima, M., Maeda, H., Hata, K., Inatomi, O., Tsujikawa, T., Sasaki, M., Takahashi, K., and Fujiyama, Y. (2005). Serum selenoprotein-P levels in patients with inflammatory bowel disease. Nutrition *21*, 574–579.

Auberger, P., Falquerho, L., Contreres, J.O., Pages, G., Le Cam, G., Rossi, B., and Le Cam, A. (1989). Characterization of a natural inhibitor of the insulin receptor tyrosine kinase: cDNA cloning, purification, and anti-mitogenic activity. Cell *58*, 631–640.

Bellinger, F.P., He, Q.P., Bellinger, M.T., Lin, Y., Raman, A.V., White, L.R., and Berry, M.J. (2008). Association of selenoprotein p with Alzheimer's pathology in human cortex. J. Alzheimers Dis. *15*, 465–472.

Bleys, J., Navas-Acien, A., and Guallar, E. (2007). Serum selenium and diabetes in U.S. adults. Diabetes Care *30*, 829–834.

Burk, R.F., and Hill, K.E. (2005). Selenoprotein P: an extracellular protein with unique physical characteristics and a role in selenium homeostasis. Annu. Rev. Nutr. *25*, 215–235.

Burk, R.F., Hill, K.E., Olson, G.E., Weeber, E.J., Motley, A.K., Winfrey, V.P., and Austin, L.M. (2007). Deletion of apolipoprotein E receptor-2 in mice lowers brain selenium and causes severe neurological dysfunction and death when a low-selenium diet is fed. J. Neurosci. *27*, 6207–6211.

Carlson, B.A., Novoselov, S.V., Kumaraswamy, E., Lee, B.J., Anver, M.R., Gladyshev, V.N., and Hatfield, D.L. (2004). Specific excision of the selenocysteine tRNA[Ser]Sec (Trsp) gene in mouse liver demonstrates an essential role of selenoproteins in liver function. J. Biol. Chem. *279*, 8011–8017.

Davies, S.P., Helps, N.R., Cohen, P.T., and Hardie, D.G. (1995). 5'-AMP inhibits dephosphorylation, as well as promoting phosphorylation, of the AMP-activated protein kinase. Studies using bacterially expressed human protein phosphatase-2C alpha and native bovine protein phosphatase-2AC. FEBS Lett. *377*, 421–425.

Després, J.P., Lamarche, B., Mauriège, P., Cantin, B., Dagenais, G.R., Moorjani, S., and Lupien, P.J. (1996). Hyperinsulinemia as an independent risk factor for ischemic heart disease. N. Engl. J. Med. *334*, 952–957.

Friedman, J.M., and Halaas, J.L. (1998). Leptin and the regulation of body weight in mammals. Nature *395*, 763–770.

Hill, K.E., Zhou, J., McMahan, W.J., Motley, A.K., Atkins, J.F., Gesteland, R.F., and Burk, R.F. (2003). Deletion of selenoprotein P alters distribution of selenium in the mouse. J. Biol. Chem. *278*, 13640–13646.

Kahn, B.B., Alquier, T., Carling, D., and Hardie, D.G. (2005). AMP-activated protein kinase: ancient energy gauge provides clues to modern understanding of metabolism. Cell Metab. *1*, 15–25.

Kawano, K., Hirashima, T., Mori, S., Saitoh, Y., Kurosumi, M., and Natori, T. (1992). Spontaneous long-term hyperglycemic rat with diabetic complications. Otsuka Long-Evans Tokushima Fatty (OLETF) strain. Diabetes *41*, 1422–1428.

Maeda, K., Okubo, K., Shimomura, I., Funahashi, T., Matsuzawa, Y., and Matsubara, K. (1996). cDNA cloning and expression of a novel adipose specific collagen-like factor, apM1 (AdiPose Most abundant Gene transcript 1). Biochem. Biophys. Res. Commun. *221*, 286–289.

Maeda, N., Shimomura, I., Kishida, K., Nishizawa, H., Matsuda, M., Nagaretani, H., Furuyama, N., Kondo, H., Takahashi, M., Arita, Y., et al. (2002). Diet-induced insulin resistance in mice lacking adiponectin/ACRP30. Nat. Med. *8*, 731–737.

Masiulis, I., Quill, T.A., Burk, R.F., and Herz, J. (2009). Differential functions of the Apoer2 intracellular domain in selenium uptake and cell signaling. Biol. Chem. *390*, 67–73.

McCaffrey, A.P., Meuse, L., Pham, T.T., Conklin, D.S., Hannon, G.J., and Kay, M.A. (2002). RNA interference in adult mice. Nature *418*, 38–39.

Minokoshi, Y., Kim, Y.B., Peroni, O.D., Fryer, L.G., Müller, C., Carling, D., and Kahn, B.B. (2002). Leptin stimulates fatty-acid oxidation by activating AMP-activated protein kinase. Nature *415*, 339–343.

Misu, H., Takamura, T., Matsuzawa, N., Shimizu, A., Ota, T., Sakurai, M., Ando, H., Arai, K., Yamashita, T., Honda, M., et al. (2007). Genes involved in oxidative phosphorylation are coordinately upregulated with fasting hyperglycaemia in livers of patients with type 2 diabetes. Diabetologia *50*, 268–277.

Oike, Y., Akao, M., Yasunaga, K., Yamauchi, T., Morisada, T., Ito, Y., Urano, T., Kimura, Y., Kubota, Y., Maekawa, H., et al. (2005). Angiopoietin-related growth factor antagonizes obesity and insulin resistance. Nat. Med. *11*, 400–408.

Olson, G.E., Winfrey, V.P., Nagdas, S.K., Hill, K.E., and Burk, R.F. (2007). Apolipoprotein E receptor-2 (ApoER2) mediates selenium uptake from selenoprotein P by the mouse testis. J. Biol. Chem. *282*, 12290–12297.

Ota, T., Takamura, T., Kurita, S., Matsuzawa, N., Kita, Y., Uno, M., Akahori, H., Misu, H., Sakurai, M., Zen, Y., et al. (2007). Insulin resistance accelerates a dietary rat model of nonalcoholic steatohepatitis. Gastroenterology *132*, 282–293.

Persson-Moschos, M., Alfthan, G., and Akesson, B. (1998). Plasma selenoprotein P levels of healthy males in different selenium status after oral supplementation with different forms of selenium. Eur. J. Clin. Nutr. *52*, 363–367.

Saito, Y., and Takahashi, K. (2002). Characterization of selenoprotein P as a selenium supply protein. Eur. J. Biochem. *269*, 5746–5751.

Saito, Y., Hayashi, T., Tanaka, A., Watanabe, Y., Suzuki, M., Saito, E., and Takahashi, K. (1999). Selenoprotein P in human plasma as an extracellular phospholipid hydroperoxide glutathione peroxidase. Isolation and enzymatic characterization of human selenoprotein p. J. Biol. Chem. *274*, 2866–2871.

Saito, Y., Watanabe, Y., Saito, E., Honjoh, T., and Takahashi, K. (2001). Production and application of monoclonal antibodies to human selenoprotein P. J. Health Sci. *47*, 346–352.

Saltiel, A.R., and Kahn, C.R. (2001). Insulin signalling and the regulation of glucose and lipid metabolism. Nature *414*, 799–806.

Scherer, P.E., Williams, S., Fogliano, M., Baldini, G., and Lodish, H.F. (1995). A novel serum protein similar to C1q, produced exclusively in adipocytes. J. Biol. Chem. *270*, 26746–26749.

Schomburg, L., Schweizer, U., Holtmann, B., Flohé, L., Sendtner, M., and Köhrle, J. (2003). Gene disruption discloses role of selenoprotein P in selenium delivery to target tissues. Biochem. J. *370*, 397–402.

Speckmann, B., Walter, P.L., Alili, L., Reinehr, R., Sies, H., Klotz, L.O., and Steinbrenner, H. (2008). Selenoprotein P expression is controlled through interaction of the coactivator PGC-1alpha with FoxO1a and hepatocyte nuclear factor 4alpha transcription factors. Hepatology *48*, 1998–2006.

Srinivas, P.R., Wagner, A.S., Reddy, L.V., Deutsch, D.D., Leon, M.A., Goustin, A.S., and Grunberger, G. (1993). Serum alpha 2-HS-glycoprotein is an inhibitor of the human insulin receptor at the tyrosine kinase level. Mol. Endocrinol. *7*, 1445–1455.

Steinberg, G.R., Michell, B.J., van Denderen, B.J., Watt, M.J., Carey, A.L., Fam, B.C., Andrikopoulos, S., Proietto, J., Görgün, C.Z., Carling, D., et al. (2006). Tumor necrosis factor alpha-induced skeletal muscle insulin resistance involves suppression of AMP-kinase signaling. Cell Metab. *4*, 465–474.

Steppan, C.M., Bailey, S.T., Bhat, S., Brown, E.J., Banerjee, R.R., Wright, C.M., Patel, H.R., Ahima, R.S., and Lazar, M.A. (2001). The hormone resistin links obesity to diabetes. Nature *409*, 307–312.

Takamura, T., Sakurai, M., Ota, T., Ando, H., Honda, M., and Kaneko, S. (2004). Genes for systemic vascular complications are differentially expressed in the livers of type 2 diabetic patients. Diabetologia *47*, 638–647.

Takeda, S., Sato, N., Uchio-Yamada, K., Sawada, K., Kunieda, T., Takeuchi, D., Kurinami, H., Shinohara, M., Rakugi, H., and Morishita, R. (2010). Diabetes-accelerated memory dysfunction via cerebrovascular inflammation and Abeta deposition in an Alzheimer mouse model with diabetes. Proc. Natl. Acad. Sci. USA *107*, 7036–7041.

Takeshita, Y., Takamura, T., Hamaguchi, E., Shimizu, A., Ota, T., Sakurai, M., and Kaneko, S. (2006). Tumor necrosis factor-alpha-induced production of plasminogen activator inhibitor 1 and its regulation by pioglitazone and cerivastatin in a nonmalignant human hepatocyte cell line. Metabolism *55*, 1464–1472.

Velculescu, V.E., Zhang, L., Vogelstein, B., and Kinzler, K.W. (1995). Serial analysis of gene expression. Science *270*, 484–487.

Walter, P.L., Steinbrenner, H., Barthel, A., and Klotz, L.O. (2008). Stimulation of selenoprotein P promoter activity in hepatoma cells by FoxO1a transcription factor. Biochem. Biophys. Res. Commun. *365*, 316–321.

Xu, A., Lam, M.C., Chan, K.W., Wang, Y., Zhang, J., Hoo, R.L., Xu, J.Y., Chen, B., Chow, W.S., Tso, A.W., and Lam, K.S. (2005). Angiopoietin-like protein 4 decreases blood glucose and improves glucose tolerance but induces hyperlipidemia and hepatic steatosis in mice. Proc. Natl. Acad. Sci. USA *102*, 6086–6091.

Yamauchi, T., Kamon, J., Minokoshi, Y., Ito, Y., Waki, H., Uchida, S., Yamashita, S., Noda, M., Kita, S., Ueki, K., et al. (2002). Adiponectin stimulates glucose utilization and fatty-acid oxidation by activating AMP-activated protein kinase. Nat. Med. *8*, 1288–1295.

Yang, Q., Graham, T.E., Mody, N., Preitner, F., Peroni, O.D., Zabolotny, J.M., Kotani, K., Quadro, L., and Kahn, B.B. (2005). Serum retinol binding protein 4 contributes to insulin resistance in obesity and type 2 diabetes. Nature *436*, 356–362.

Zender, L., Hutker, S., Liedtke, C., Tillmann, H.L., Zender, S., Mundt, B., Waltemathe, M., Gosling, T., Flemming, P., Malek, N.P., et al. (2003). Caspase 8 small interfering RNA prevents acute liver failure in mice. Proc. Natl. Acad. Sci. USA *100*, 7797–7802.

Research Article

EASL EUROPEAN ASSOCIATION FOR THE STUDY OF THE LIVER | JOURNAL OF HEPATOLOGY

Differential interferon signaling in liver lobule and portal area cells under treatment for chronic hepatitis C

Masao Honda[1,2], Mikiko Nakamura[1], Makoto Tateno[1], Akito Sakai[1], Tetsuro Shimakami[1], Takayoshi Shirasaki[1], Tatsuya Yamashita[1], Kuniaki Arai[1], Taro Yamashita[1], Yoshio Sakai[1], Shuichi Kaneko[1,*]

[1]*Department of Gastroenterology, Kanazawa University, Graduate School of Medicine, Kanazawa, Japan;* [2]*Department of Advanced Medical Technology, Kanazawa University, Graduate School of Health Medicine, Kanazawa, Japan*

Background & Aims: The mechanisms of treatment resistance to interferon (IFN) and ribavirin (Rib) combination therapy for hepatitis C virus (HCV) infection are not known. This study aims to gain insight into these mechanisms by exploring hepatic gene expression before and during treatment.

Methods: Liver biopsy was performed in 50 patients before therapy and repeated in 30 of them 1 week after initiating combination therapy. The cells in liver lobules (CLL) and the cells in portal areas (CPA) were obtained from 12 patients using laser capture microdissection (LCM).

Results: Forty-three patients were infected with genotype 1 HCV, 20 of who were viral responders (genotype 1-Rsp) with treatment outcome of SVR or TR, while 23 were non-responders (genotype 1-nonRsp) with NR. Only seven patients were infected with genotype 2. Before treatment, the expression of *IFN and Rib-stimulated genes* (IRSGs), apoptosis-associated genes, and immune reaction gene pathways was greater in genotype 1-nonRsp than in Rsp. During treatment, IRSGs were induced in genotype 1-Rsp, but not in nonRsp. IRSG induction was irrelevant in genotype 2-Rsp and was mainly impaired in CLL but not in CPA. Pathway analysis revealed that many immune regulatory pathways were induced in CLL from genotype 1-Rsp, while growth factors related to angiogenesis and fibrogenesis were more induced in CPA from genotype 1-nonRsp.

Conclusions: Impaired IRSGs induction in CLL reduces the sensitivity to treatment for genotype 1 HCV infection. CLL and CPA in the liver might be differentially involved in treatment resistance. These findings could be useful for the improvement of therapy for HCV infection.

Introduction

A human liver infected with hepatitis C virus (HCV) develops chronic hepatitis, cirrhosis, and in some instances, hepatocellular carcinoma (HCC). Although interferon (IFN) and ribavirin (Rib) combination therapy has become a popular modality for treating patients with chronic hepatitis C (CH-C), about 50% of patients relapse, particularly those with genotype 1b and high viral load [8]. The reasons for treatment failure are poorly understood. Many studies of IFN and Rib combination therapy for CH-C suggested that patients who cleared HCV viremia early during therapy tended to show favorable outcomes. On the other hand, patients who needed a longer period to clear HCV had poorer outcomes [4,7,17], and those who showed no response (no or minimal decrease in HCV-RNA) to IFN and Rib combination therapy hardly ever achieved a sustained viral response (SVR).

To elucidate the underlying mechanism of treatment resistance, expression profiles in the liver [3,6,20] and peripheral mononuclear cells (PBMC) [10,21] during IFN treatment for CH-C patients have been examined. In chronic viral hepatitis, increased numbers of immune regulatory cells infiltrate the liver. These liver-infiltrating lymphocytes (LILs) might play important roles for virus eradication and are potentially linked to treatment outcome. Previously, we selectively isolated cells in liver lobules (CLL) and cells in the portal area (CPA) from biopsy specimens using laser capture microdissection (LCM) and analyzed their gene expression profiles [11,19]. From these profile analyses, it could be inferred that the majority of CLL were hepatocytes and the majority of CPA were lymphocytes, although other cellular components such as Kupffer cells, endothelial cells, myofibroblasts, and bile duct cells co-existed as well.

To gain further insight into the mechanisms of therapy resistance, we analyzed expression profiles in CLL and CPA in addition to whole liver tissues during IFN therapy for CH-C.

Keywords: HCV; IFN; LCM; Gene expression.
Received 12 October 2009; received in revised form 29 April 2010; accepted 30 April 2010; available online 15 July 2010

* Corresponding author. Address: Department of Gastroenterology, Kanazawa University, Graduate School of Medicine, Takara-Machi 13-1, Kanazawa 920-8641, Japan. Tel.: +81 76 265 2235; fax: +81 76 234 4250.
E-mail address: skaneko@m-kanazawa.jp (S. Kaneko).

Abbreviations: HCV, hepatitis C virus; HBV, hepatitis B virus; miRNA, micro RNA; CH-B, chronic hepatitis B; CH-C, chronic hepatitis C; HCC-B, hepatitis B-related hepatocellular carcinoma; HCC-C, hepatitis C-related hepatocellular carcinoma; OCT, optimum cutting temperature.

Research Article

Materials and methods

Patients

Patients with CH-C were enrolled in this study at the Graduate School of Medicine, Kanazawa University Hospital, Japan, between 2001 and 2007 (Tables 1 and 2). Prior to the study, we obtained the required approvals, namely: informed consent from all participating patients and ethics approval from the ethics committee for human genome/gene analysis research at Kanazawa University Graduate School of Medical Science. Thirty patients were administered IFN-α 2b (6 MU: every day for 2 weeks, then three times a week for 22 weeks) (Schering-Plough K.K., Tokyo, Japan) and Rib (10–13 mg/kg/day) combination therapy for 24 weeks (Table 1). Twenty patients were administered Peg-IFN-α 2b and Rib combination therapy for 48 weeks (Table 2). The final outcome of the treatment was assessed at 24 weeks after cessation of the combination therapy. In addition, 10 samples of normal liver tissues obtained during surgery for metastatic liver cancer were used as controls.

We defined treatment outcomes according to the decrease in viremia as follows: sustained viral response (SVR), clearance of HCV viremia at 24 weeks after cessation of therapy; transient response (TR), no detectable HCV viremia at 24 weeks but relapse during the follow-up period; and nonresponse (NR), HCV viremia detected at the cessation of therapy. We defined a patient who achieved SVR or TR as a viral responder (Rsp) and a patient who exhibited an NR as a nonresponder (nonRsp). As patient 10 stopped treatment at 5 weeks due to an adverse side effect, we grouped this patient as Rsp based on the observed viral decline within 2 weeks (Table 1).

HCV genotype was classified by the methods described by Okamoto et al. [16] Twenty-three patients were infected with genotype 1b and seven patients were infected with genotype 2 (2a; 6, 2b; 1) (Tables 1 and 2).

Patient serum was aliquoted and stored at −20 °C until use. HCV-RNA was serially monitored by quantitative real-time detection (RTD)-PCR (COBAS® AmpliPrep/COBAS® TaqMan® System®) [9] before treatment, at 48 h, 2 weeks and 24 weeks after initiation of therapy and at 24 weeks after cessation of therapy.

The grading and staging of chronic hepatitis were histologically assessed according to the method described by Desmet et al. (Table 1) [5].

Table 1. Characteristics of study patients who received IFN and ribavirin combination therapy.

				ALT (IU/ml)		Liver histology			HCV-RNA (Log IU/ml)				Viral kinetics			
Pt.No.	Sex	Age (yr)	Genotype	Before therapy	During therapy	Before therapy F A	During therapy F A	LCM	Before therapy	48 h	2 wk	24 wk	1st phase delinie Log/24 h	2nd phase decline Log/week	Viral response	Outcome
1	M	48	1b	83	45	1 1	1 1	+	6.6	4.5	3.5	-	1.1	0.5	Rsp	SVR
2	M	32	1b	192	95	1 1	1 1	-	6.4	3.9	3.2	-	1.3	0.4	Rsp	SVR
3	F	50	1b	57	37	1 1	1 1	-	5.8	2.5	1.5	-	1.7	0.5	Rsp	TR
4	M	36	1b	119	117	1 1	1 1	+	6.1	4.4	4.2	+	0.9	0.1	nonRsp	NR
5	M	54	1b	82	69	1 1	1 1	-	6.6	5.1	3.9	+	0.8	0.6	nonRsp	NR
6	M	43	1b	143	116	1 1	1 1	-	6.3	4.4	4.1	+	1.0	0.2	nonRsp	NR
7	M	48	1b	33	30	1 1	1 1	+	1.5	0.0	0.0	-	>0.8	-	Rsp	SVR
8	M	52	1b	316	374	1 2	1 1	-	4.7	5.1	3.9	+	-0.2	0.6	nonRsp	NR
9	M	45	1b	112	39	1 0	2 0	-	6.2	5.1	5.7	+	0.6	-0.3	nonRsp	NR
10	M	48	1b	48	30	2 2	2 1	+	6.4	4.0	2.6	NA	1.2	0.8	Rsp	NA
11	M	52	1b	114	80	2 2	2 1	-	6.1	3.7	3.0	-	1.2	0.4	Rsp	TR
12	F	63	1b	38	30	2 1	2 1	-	5.2	4.2	4.5	+	0.5	-0.2	nonRsp	NR
13	M	58	1b	90	83	2 2	2 2	+	6.9	4.9	5.6	+	1.0	-0.4	nonRsp	NR
14	F	61	1b	87	43	2 1	2 1	+	6.5	3.9	3.7	+	1.3	0.1	nonRsp	NR
15	F	64	1b	133	111	2 1	3 2	-	6.0	4.4	3.6	+	0.8	0.4	nonRsp	NR
16	F	62	1b	251	159	3 2	3 2	-	4.8	2.7	1.5	-	1.1	0.6	Rsp	SVR
17	M	54	1b	211	205	3 2	3 2	+	6.7	0.0	0.0	-	>3.4	-	Rsp	SVR
18	F	68	1b	153	145	3 2	3 2	+	4.9	4.3	3.5	+	0.3	0.4	nonRsp	NR
19	F	69	1b	64	43	3 2	3 2	-	4.4	1.5	0.0	-	1.5	0.8	Rsp	SVR
20	M	49	1b	91	83	3 2	3 2	+	6.6	4.2	3.8	+	1.2	0.2	nonRsp	NR
21	M	55	1b	187	196	4 1	4 2	-	5.8	5.1	5.6	+	0.4	-0.3	nonRsp	NR
22	F	45	1b	113	75	4 2	3 3	-	5.7	4.2	2.7	-	0.8	0.8	Rsp	TR
23	M	60	1b	86	49	4 2	3 1	-	6.3	3.5	3.5	+	1.4	0.0	nonRsp	NR
24	F	51	2b	98	90	1 1	1 1	-	2.7	1.5	0.0	-	0.6	0.8	Rsp	SVR
25	M	37	2a	241	211	1 0	1 0	-	4.0	1.5	0.0	-	1.3	0.8	Rsp	SVR
26	F	45	2a	91	33	2 1	2 1	-	5.4	2.2	1.5	-	1.6	0.4	Rsp	TR
27	M	46	2a	101	45	2 1	2 1	+	3.6	0.0	0.0	-	>1.8	-	Rsp	SVR
28	M	54	2a	196	177	3 2	2 1	+	4.2	0.0	0.0	-	>2.1	-	Rsp	SVR
29	F	68	2a	234	135	3 1	3 2	+	4.6	3.1	0.0	-	0.8	1.7	Rsp	SVR
30	M	67	2a	155	163	4 2	4 2	-	3.9	1.5	0.0	-	1.2	0.8	Rsp	SVR

First phase decline was determined by subtracting HCV-RNA at 48 h from before therapy.
Second phase decline was determined by subtracting HCV-RNA at 2 wk from 48 h.
NA, not applicable; LCM, laser capture microdissection; ALT, alanine aminotransferase; SVR, sustained viral response; A, activity; NR, nonresponse; F, fibrosis; TR, transient response; Rsp, viral responder, patients with SVR or TR; nonRsp, non-viral responder; patients with NR; HCV-RNA was assayed by COBAS® AmpliPrep/COBAS® TaqMan® System® (Log IU/mL).

Table 2. Characteristics of patients who received Peg-IFN and ribavirin combination therapy and normal control.

Pt.No.	Sex	Age (yr)	Genotype	ALT (IU/ml)	Liver histology		HCV-RNA (Log IU/ml)				Viral response	Outcome
				Before therapy	Before therapy		Before therapy	2 wk	4 wk	24 wk		
					F	A						
1	M	57	1b	68	1	1	6.5	-	-	-	Rsp	SVR
2	F	56	1b	31	1	1	6.5	4.4	-	-	Rsp	SVR
3	M	63	1b	50	1	1	6.1	-	-	-	Rsp	SVR
4	M	44	1b	45	1	1	6.5	3.7	-	-	Rsp	SVR
5	F	51	1b	27	2	1	6.5	4.1	-	-	Rsp	SVR
6	M	58	1b	72	2	1	6.2	-	-	-	Rsp	SVR
7	M	60	1b	71	2	2	6.2	3.9	-	-	Rsp	SVR
8	F	52	1b	58	2	2	6.5	4.1	-	-	Rsp	SVR
9	F	62	1b	60	3	2	5.9	3.8	-	-	Rsp	SVR
10	M	55	1b	106	3	2	6.4	-	-	-	Rsp	SVR
11	M	30	1b	31	1	1	6.4	6.1	5.9	+	nonRsp	NR
12	F	55	1b	23	1	2	6.5	6.1	5.9	+	nonRsp	NR
13	M	58	1b	129	1	2	6.3	6.0	5.8	+	nonRsp	NR
14	M	42	1b	326	2	1	6.6	6.2	5.8	+	nonRsp	NR
15	F	61	1b	77	2	1	6.1	5.9	5.7	+	nonRsp	NR
16	F	44	1b	31	2	2	5.5	5.3	4.7	+	nonRsp	NR
17	M	51	1b	38	2	2	6.5	6.2	5.9	+	nonRsp	NR
18	F	55	1b	97	2	2	6.7	6.3	6.1	+	nonRsp	NR
19	M	59	1b	31	3	2	6.7	5.9	5.7	+	nonRsp	NR
20	F	53	1b	71	3	2	5.9	5.8	5.8	+	nonRsp	NR
21	F	51	-	18	0	0	-	-	-	-	-	-
22	F	78	-	13	0	0	-	-	-	-	-	-
23	M	75	-	20	0	0	-	-	-	-	-	-
24	M	34	-	12	0	0	-	-	-	-	-	-
25	M	64	-	30	0	0	-	-	-	-	-	-
26	M	78	-	9	0	0	-	-	-	-	-	-
27	M	53	-	19	0	0	-	-	-	-	-	-
28	F	64	-	12	0	0	-	-	-	-	-	-
29	F	60	-	20	0	0	-	-	-	-	-	-
30	M	66	-	26	0	0	-	-	-	-	-	-

SVR, sustained viral response; NR, nonresponse; Rsp, viral responder, patients with SVR or TR; nonRsp, non-viral responder; patients with NR.

Preparation of liver tissue samples

Liver biopsy samples were taken from all the patients at around 1 week before treatment and at 1 week after starting therapy (Fig. 1A). The biopsy samples were divided into three parts: the first part was immersed in formalin for histological assessment, the second was immediately frozen in liquid nitrogen tank for future RNA isolation, and the final part was frozen in OCT compound for LCM analysis and stored at −80 °C until use. As a control, a liver tissue sample was surgically obtained from a patient who showed no clinical signs of hepatitis and was analyzed as described previously [11].

CLL and CPA were isolated by LCM using a CRI-337 (Cell Robotics, Albuquerque, NM, USA) (Supplementary Fig. 1) from the liver biopsy specimens frozen in OCT compound. The detailed procedure for LCM is described in the Supplementary materials and methods and was performed as previously described [11,19].

RNA isolation and Affymetrix gene chip analysis

Total RNA in each liver biopsy specimen was isolated using the RNAqueous® kit (Ambion, Austin, TX, USA). Total RNA in the specimens frozen for LCM was isolated with a carrier nucleic acid (20 ng poly C) using RNAqueous®-Micro (Ambion). The quality of the isolated RNA was estimated after electrophoresis using an Agilent 2001 Bioanalyzer (Palo Alto, CA, USA). Aliquots of total RNA (50 ng) isolated from the liver biopsy specimens were subjected to amplification with the WT-Ovation™ Pico RNA Amplification System (NuGen, San Carlos, CA, USA) as recommended by the manufacturer. About 10 μg of cDNA was amplified from 50 ng total RNA, and 5 μg of cDNA was used for fragmentation and biotin labeling using the FL-Ovation™ cDNA Biotin Module V2 (NuGen) as recommended by the manufacturer. The biotin-labeled cDNA was suspended in 220 μl of hybridization cocktail (NuGen), and 200 μl was used for the hybridization. Half of the total RNA isolated from the LCM specimens was amplified twice with the TargetAmp™ 2-Round Aminoallyl-aRNA Amplification Kit 1.0 (EPICENTRE, Madison, WI, USA). Twenty-five micrograms of amplified antisense RNA were used for biotin labeling according to the manufacturer's protocol *Biotin-X-X-NHS* (provided by EPICENTRE). The biotin-labeled aRNA was suspended in 300 μl of hybridization cocktail (Affymetrix Inc., Santa Clara, CA, USA), and 200 μl was used for the hybridization with the Affymetrix Human 133 Plus 2.0 microarray chip containing 54,675 probes. After stringent washing, the microarray chips were stained with streptavidin–phycoerythrin, and probe hybridization was determined using a GeneChip® Scanner 3000 (Affymetrix). Data files (CEL) were obtained with the GeneChip® Operating Software 1.4 (GCOS) (Affymetrix). All the expression data were deposited in Gene Expression Omunibus (GEO; http://www.ncbi.nlm.nih.gov/geo/) (NCBI) and the accession ID is GSM 425,995. The experimental procedure is described in detail in the Supplementary materials and methods.

Research Article

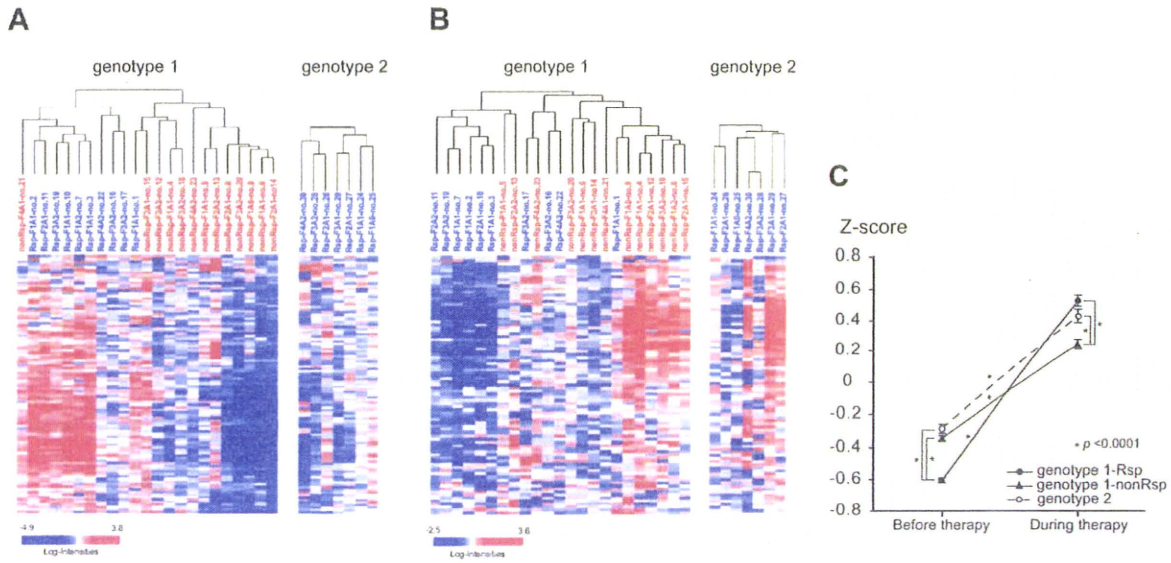

Fig. 1. (A) Hierarchical clustering of expression in genotype 1 and genotype 2 patients during treatment according to fold induction of IRSGs. (B) Hierarchical clustering of expression in genotype 1 and genotype 2 patients before treatment. (C) Serial changes in standardized expression values (Z-score) of IRSGs from genotype 1-Rsp, genotype 1-nonRsp, and genotype 2 patients before and during treatment.

Statistical and pathway analysis of gene chip data

Statistical analysis and hierarchical clustering were performed by BRB-ArrayTools (http://linus.nci.nih.gov/BRB-ArrayTools.htm). A class comparison tool based on univariate or paired *t*-tests was used to find differentially expressed genes (p <0.005). To confirm statistical significance, 2000 random permutations were performed, and all of the *t*-tests were re-computed for each gene. The gene set comparison was analyzed using the BioCarta and the KEGG pathway data bases. The Fisher and Kolmogorov–Smirnov tests were performed for statistical evaluation (p <0.005) (BRB-ArrayTools). Functional ontology enrichment analysis was performed to compare the Gene Ontology (GO) process distribution of differentially expressed genes (p <0.05) using MetaCore™ (GeneGo, St. Joseph, MI, USA).

For the comparison of standardized expression values among different pathway groups, standard units (Z-score) of each gene expression value were calculated as:

$$Z_i = \frac{X_i - X_m}{S}$$

where X_i is the raw expression value, X_m is the mean of the expression values in the pathway, and S is the standard deviation of the expression values.

The standard units in each pathway were expressed as mean ± SEM. A *P*-value of less than 0.05 was considered significant. Multivariate analysis was performed using a logistic regression model with a stepwise method using JMP7 for Windows (SAS Institute, Cary, NC, USA).

Quantitative real-time detection (RTD)-PCR

We performed quantitative real-time detection PCR (RTD)-PCR using TaqMan Universal Master Mix (PE Applied Biosystems, CA). Primer pairs and probes for Mx1, IFI44 and IFITM1, and GAPDH were obtained from TaqMan assay reagents library (Applied Biosystems, CA).

Results

Serial changes in HCV-RNA after initiation of IFN-α 2b and Rib combination therapy

Serial changes in HCV-RNA were monitored at 48 h, 2 weeks, and 24 weeks after the initiation of therapy (Table 1). The biphasic viral decline after the initiation of IFN therapy has been characterized [14,15,18]. We calculated the first phase decline by comparing viral load before therapy and after 48 h, and the second phase decline by comparing viral load after 48 h and 2 weeks (Table 1) [14,15,18]. Both the first and the second phase declines could be associated with treatment outcome and interestingly, viral responders (Rsp) who achieved SVR or TR showed more than a 1-log drop of first phase decline (Log/24 h) and more than a 0.3-log drop of second phase decline (Log/w) (Table 1). In contrast, non-responders (nonRsp) who exhibited NR failed to meet the criteria. The first phase decline of Rsp and nonRsp were 1.38 ± 0.65 log/24 h and 0.77 ± 0.44 log/24 h (p = 0.005), respectively. The second phase decline of Rsp and nonRsp were 0.71 ± 0.34 log/w and 0.11 ± 0.34 log/w (p = 0.0001), respectively. Therefore, the classification of Rsp or nonRsp according to the treatment outcome might be feasible based on the viral kinetic responses to IFN. All but one patient infected with genotype 2 HCV eliminated the virus within 2 weeks. There were no significant differences in the degree of histological activity or staging, nor in the sex, age, or alanine aminotransferase (ALT) level among these patients (Table 1). The amount of HCV-RNA was significantly lower in genotype 2 patients (4.06 ± 0.32 log IU/ml) than in genotype 1 patients (5.70 ± 1.10 log IU/ml) (Table 1).

Identification of IFN-α 2b plus Rib-induced genes in the livers of patients with chronic hepatitis C infection

To identify the genes induced in the liver by combination treatment with IFN-α 2b plus Rib, the gene expression profiles from samples taken around 1 week before and 1 week after initiation of therapy were compared. The pairwise *t*-test comparison showed that 798 genes were up-regulated and 220 genes were down-regulated significantly (p <0.005). The 100 most up-regulated genes according to p values were selected; these are listed in Supplementary Table 1. Many of the interferon-stimulated

genes (ISGs), such as Myxovirus (influenza virus) resistance 1 (MX), 2′,5′-oligoadenylate synthetase (OAS), chemokine (C–C motif) ligand 8 (CCL8), and interferon alpha-inducible protein 27 (IFI 27), were significantly induced (Supplementary Table 1). We designated these genes as *IFN and Rib-stimulated genes* (IRSGs) and analyzed them further.

Hepatic gene expression and responsiveness to IFN-α 2b and Rib combination therapy

To investigate the relationship between hepatic gene expression and responsiveness to treatment, we applied nonsupervised learning methods, hierarchical clustering analysis using all the expressed genes ($n = 34{,}988$) from samples taken before and 1 week after initiation of therapy. While hierarchical clustering analysis did not form clusters when done for all patients, it formed two clusters – Rsp and nonRsp – when performed within genotype 1 patient (data not shown).

Fold changes in expression in the 100 most up-regulated IRSGs, before and during therapy, were calculated and subjected to hierarchical clustering, and this clearly differentiated Rsp, which exhibited higher IRSGs induction, from nonRsp, as shown in Fig. 1A and Supplementary Table 1. Despite the rapid virus decline in genotype 2 patients, IRSG induction was not so evident in these patients.

Unexpectedly, the hierarchical clustering of IRSG expression in samples taken before treatment showed a reverse pattern of gene expression (Fig. 2B): IRSG induction was significantly higher in nonRsp than in Rsp. Upon treatment, the expression of IRSGs was more induced in Rsp than in nonRsp (Fig. 1C).

The findings were confirmed in patients who were administered Peg-IFN-α 2b and Rib combination therapy (Table 2). IRSG expression was induced in CH-C infected livers and substantially up-regulated in nonRsp compared with Rsp (Supplementary Fig. 1). Multivariate logistic analysis including age, sex, fibrosis stage, activity, HCV-RNA, genotype, treatment regime, ALT and

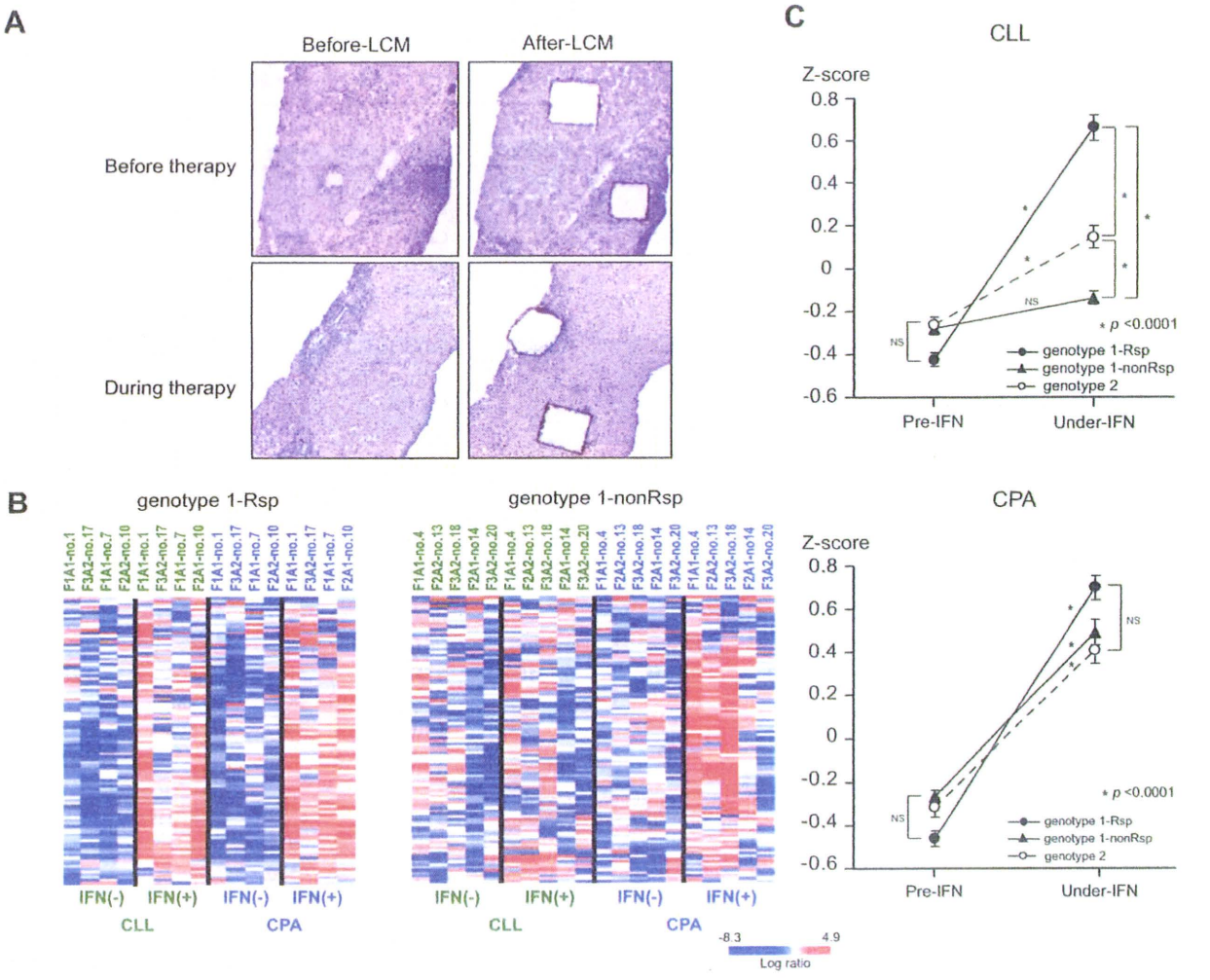

Fig. 2. (A) LCM of liver biopsy samples before and during treatment. (B) Heat map of gene expression of IRSGs in CLL and CPA before and during treatment. (C) Serial changes in standardized expression values (Z-score) of IRSGs in CLL and CPA from genotype 1-Rsp, genotype 1-nonRsp, and genotype 2 patients before and during treatment.

expression pattern of IRSGs (up or down) of the 50 patients before treatment showed that genotype 2 (p <0.0001, Odds = 4×10^7) and down-regulated IRSGs (p <0.0001, Odds = 71.2) are significant variables associated with SVR.

Gene expression analysis in cells in liver lobules (CLL) and portal area (CPA)

To explore these findings in more detail, we examined the gene expression profiles of CLL and CPA that had been isolated separately from whole liver biopsy specimens of 12 patients, using the LCM method before and during treatment (Fig. 2A). The representative differentially expressed genes between CLL and CPA are shown in Supplementary Tables 2-1 and 2-2. In CLL, liver-specific proteins and enzymes, such as cytochrome P450, apolipoprotein, and transferrin, were all expressed. In CPA, cytokines, chemokines and lymphocyte surface markers, such as chemokine (C–X–C motif) receptor 4, interleukin-7 receptor and CD83 antigen, were all expressed (Supplementary Tables 2-1 and 2-2). The results confirmed our previous speculation that cells from the lobular area were mostly of hepatocyte origin and that those from the portal area were mostly of liver-infiltrating lymphocyte origin [11,19].

IRSG expression in CLL and CPA from genotype 1-Rsp and non-Rsp is shown in Fig. 2B. In genotype 1-Rsp, IRSG expression was significantly induced in both CLL and CPA by the treatment (Fig. 2B and C). On the other hand, in genotype 1-nonRsp and genotype 2, IRSG induction was impaired especially in CLL, while

Table 3. Up- and down-regulated pathways by gene set comparison between Rsp and nonRsp of genotype 1 patients before therapy (BRB-array tool).

Pathway	No. of genes	LS p value	KS p value	Representative Genes	Mean probe intensity of representative genes		
					Rsp (n = 20)	nonRsp (n = 23)	Normal (n = 10)
Up-regulated in slow viral drop							
IFN alpha signaling pathway	21	0.00001	0.00300	STAT1	1608	3117	686
				IRF9	1249	1842	614
				IFNAR2	1892	1988	903
Apoptotic Signaling in Response to DNA Damage	55	0.00001	0.07974	CASP3	675	870	426
				CASP7	1165	1510	1264
				CASP9	355	403	264
				TP53	1465	1797	1028
Toll-like receptor signaling pathway	150	0.00006	0.06659	CXCL10	1922	3979	193
				CXCL11	176	321	51
				MYD88	1022	1372	723
				TIRAP	582	722	447
Wnt signal pathway	55	0.00009	0.16058	EIF2AK2	664	1190	484
				CCND1	2439	3558	1162
				APC	143	186	154
				PIK3R1	1570	1906	682
Antigen processing and presentation	139	0.00117	0.00091	TAP2	169	317	93
				HLA-A	11005	14726	6221
				HLA-B	13144	17942	6823
				HLA-C	1937	3993	783
Jak-STAT signaling pathway	220	0.00180	0.13154	STAT2	716	1065	274
				IL28RA	390	544	204
				IL10RB	398	506	338
Down-regulated in slow viral drop							
Metabolism of xenobiotics by cytochrome P450	98	0.00018	0.00082	CYP3A4	15219	10118	19256
				CYP2E1	29129	24549	30929
				AKR1C4	6126	4898	6671
Fatty acid metabolism	88	0.00480	0.05373	ACADL	826	687	785
				ALDH2	18325	16337	21844
				HSD17B4	9619	8807	10653
				ACAD11	6858	6238	8279
				ACOX1	6988	5862	8279

No. of genes, the number of genes comprising the pathway, Rsp, viral responder, patients with SVR or TR; nonRsp, non-viral responder; patients with NR.

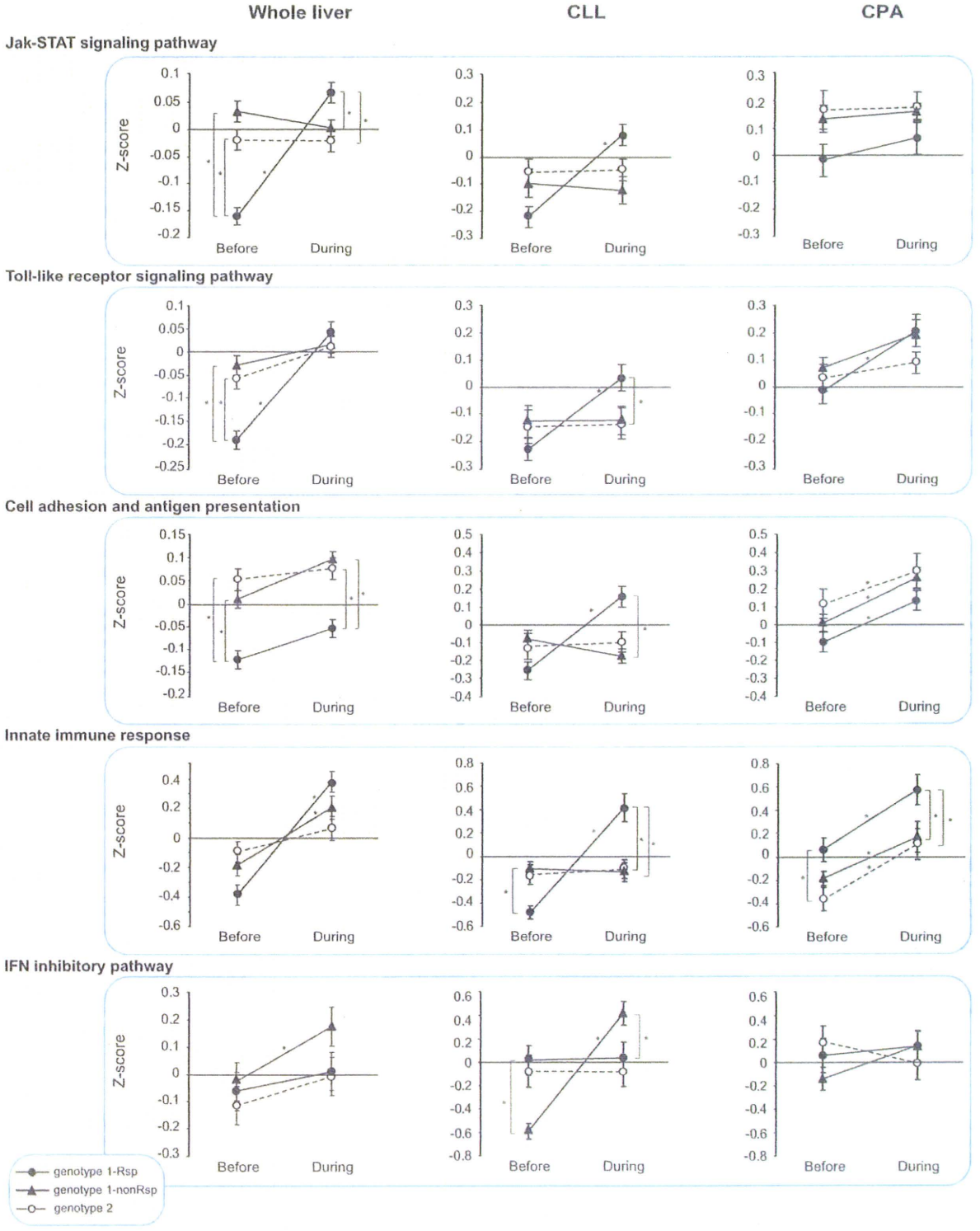

Fig. 3. Serial changes in standardized expression values (Z-score) of differentially expressed pathways from genotype 1-Rsp, genotype 1-nonRsp, and genotype 2 patients before and during treatment in whole liver, CLL, and CPA.